

The objective of this work is to determine the portion of heat flux flowing to the workpiece and the best heat distribution. For this, an inverse procedure based on the Particle Swarm Optimization was used to minimize the error between the experimental and simulated results. A finite element model that considers a preexisting hole was used to calculate the numerical temperatures. Four different heat flux distributions were analyzed and the results for each one were compared.

Advisor: Joel Martins Crichigno Filho

Joinville, 2017

YEAR
2017

JOSÉ CARLOS MEDEIROS | INVERSE IDENTIFICATION OF HEAT FLUX
IN DRY DRILLING PROCESS USING PARTICLE SWARM OPTIMIZATION



UDESC

SANTA CATARINA STATE UNIVERSITY - UDESC
COLLEGE OF TECHNOLOGICAL SCIENCE - CCT
MASTER IN MECHANICAL ENGINEERING - PPGE

MASTER THESIS

**INVERSE IDENTIFICATION OF HEAT
FLUX IN DRY DRILLING PROCESS
USING PARTICLE SWARM OPTIMIZATION**

JOINVILLE, 2017

José Carlos Medeiros

Inverse Identification of Heat Flux in Dry Drilling Process Using Particle Swarm Optimization

Master thesis presented to the Mechanical Engineering Department at the College of Technological Sciences of the Santa Catarina State University, in fulfilment of the partial requirement for the degree of Master in Mechanical Engineering

Advisor: Joel Martins Crichigno Filho

**Joinville, Brasil
2017**

Medeiros, José Carlos
Inverse Identification of Heat Flux In Dry
Drilling Process Using Particle Swarm Optimization
/ José Carlos Medeiros. - Joinville , 2018.
101 p.

Orientador: Joel Martins Crichigno Filho
Dissertação (Mestrado) - Universidade do Estado de
Santa Catarina, Centro de Ciências Tecnológicas,
Programa de Pós-Graduação em Engenharia Mecânica,
Joinville, 2018.

1. Dry Drilling. 2. Temperature. 3. Heat Flux.
4. Heat Inverse Problem. 5. PSO. I. Crichigno
Filho, Joel Martins. II. Universidade do Estado de
Santa Catarina. Programa de Pós-Graduação. III.
Título.

**Inverse Identification of Heat Flux in Dry Drilling Process Using Particle Swarm
Optimization**

por

José Carlos Medeiros

Esta dissertação foi julgada adequada para obtenção do título de

MESTRE EM ENGENHARIA MECÂNICA

Área de concentração em "Projeto, Análise e Otimização de Sistemas Mecânicos"
e aprovada em sua forma final pelo

CURSO DE MESTRADO ACADÊMICO EM ENGENHARIA MECÂNICA
CENTRO DE CIÊNCIAS TECNOLÓGICAS DA
UNIVERSIDADE DO ESTADO DE SANTA CATARINA.

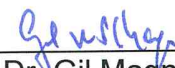
Banca Examinadora:



Prof. Dr. Joel Martins Crichigno Filho
CCT/UDESC (Orientador/Presidente)



Prof. Dr. Roberto Wolf Francisco Junior
CCT/UDESC



Prof. Dr. Gil Magno Portal Chagas
IFSC

Joinville, SC, 15 de dezembro de 2017.

ACKNOWLEDGEMENTS

First, I want to thank God for enlightening me and guiding me. To the Santa Catarina State University (UDESC) and to the Graduate Program in Mechanical Engineering for the opportunities of improvement.

To Professor Joel Martins Crichigno Filho for the guidance, support, and confidence offered throughout the development of the work. Also, thank you for all the conversations that we could have not only related to the research.

To the technician Charles Costa for the aid in the experiments developed in the laboratory and for all the good conversations.

To Douglas Negri, Felipe Klein, Ademar Bender, Leandro Perão, Douglas Pontes, Felipe Basso and João Bortolanza for their friendship and for their support in research.

To Marciane Knies, Pedro Otero, Gustavo, Mateus, Eduardo, Julia, Natalia, João among other participants of the University Prayer Group Strength in Jesus for friendship and prayers.

To my family, especially my mother Silmara, for all the support and understanding throughout the research.

*“Nothing would be done at all, if
a man waited till he could do it
so well, that no one could find
fault with it.”*

Blessed John Henry Cardinal
Newman

ABSTRACT

MEDEIROS, José Carlos. **Inverse Identification of Heat Flux in Dry Drilling Process Using Particle Swarm Optimization**. 101 pages. Master Thesis (Post Graduation Program in Mechanical Engineering) - Santa Catarina State University, Joinville, 2018.

Due to economic, environmental and health issues the use of cutting fluid has been restricted in the industry in recent years. As the cutting fluid has a cooling function, the absence of this type of product makes the thermal deformations a critical factor in dry machining. Within the drilling, this is even more problematic, as the enclosure of the tool makes the heat dissipation generated more difficult. Identification of process heat flux and temperature distributions on the workpiece allows a better understanding of the process and opens the possibility for improvements. In this context, the objective of this work is to determine the best distribution of heat flux that flows to the workpiece. For this, an inverse procedure based on the Particle Swarm Optimization was used to minimize the error between the experimental and simulated results. A hole was made in a cylindrical 1020 steel workpiece and the temperature was measured with thermocouples. Later, this piece was modeled using the ABAQUS commercial software. Using the finite element method, the workpiece was modeled considering the hole as preexisting, this simplifies the model and decreases the computational cost. Four different models of heat flux distribution for the workpiece were studied. All the approach used was satisfactory, simplifications in the simulation did not affect the results. Among the distributions proposed in the work, the hybrid was the one that obtained the smallest errors. It was also shown the importance of considering the heat flux along the machined wall, different from the classical approach which considers heat only at the tip of the drill.

Key-words: Dry Drilling. Temperature. Heat Flux. Heat Inverse Problem. PSO.

RESUMO

MEDEIROS, José Carlos. **Identificação Inversa do Fluxo de Calor no Processo de Furação a Seco utilizando Otimização por Enxame de Partículas**. 99 páginas. Dissertação (Programa de Pós Graduação em Engenharia Mecânica) - Universidade do Estado de Santa Catarina, Joinville, 2018.

Devido a questões econômicas, ambientais e de saúde o uso de fluido de corte tem sido restringido na indústria nos últimos anos. Como o fluido de corte tem função refrigerante, a ausência desse tipo de produto transforma as deformações térmicas num fator crítico dentro da usinagem a seco. Dentro da furação isto é ainda mais problemático, pois o enclausuramento da ferramenta torna a dissipação do calor gerado mais difícil. A identificação do fluxo de calor do processo e das distribuições de temperatura na peça de trabalho permitem o melhor entendimento do processo e abrem a possibilidade para melhorias. Neste contexto, o objetivo deste trabalho é o de determinar a melhor distribuição de fluxo de calor que flui para a peça. Para isto foi utilizado um procedimento inverso que utiliza a Otimização por Enxame de Partículas para minimizar o erro entre os dados experimentais e simulados. Um furo foi realizado em uma peça cilíndrica de aço 1020 e a temperatura da peça foi medida com auxílio de termopares. Posteriormente, esta peça foi modelada utilizando o software comercial ABAQUS. Utilizando o método dos elementos finitos, a peça foi modelada considerando o furo como pré-existente, isto simplifica o modelo e diminui o custo computacional. Quatro diferentes modelos de distribuição do fluxo de calor para a peça foram estudados. Toda a abordagem utilizada mostrou-se satisfatória, as simplificações na simulação não prejudicaram os resultados. Entre as distribuições propostas no trabalho, a híbrida é a que obteve os menores erros. Foi mostrado também a importância de considerar o fluxo de calor ao longo da parede usinada, diferente da abordagem clássica que considera o calor somente na ponta da broca.

Palavras-chave: Furação a Seco. Temperatura. Fluxo de Calor. Problema Inverso de Calor. PSO.

List of Figures

Figure 1 – Geometry of a spiral drill point	5
Figure 2 – Nozzle system	6
Figure 3 – Different heat-generation regions in the cutting zone	9
Figure 4 – The drill point and the orthogonal element model	11
Figure 5 – Workpiece finite element mesh	13
Figure 6 – PSO diagram	19
Figure 7 – Machine tool used in research	22
Figure 8 – Tool used in research	22
Figure 9 – Thermocouples' positions	23
Figure 10 – National Instruments Module	23
Figure 11 – Experimental setup	24
Figure 12 – 2-D axisymmetric finite element mesh	27
Figure 13 – Thermal problem	28
Figure 14 – Concentrated distribution of heat flux	33
Figure 15 – Linear distribution of heat flux	34
Figure 16 – Polynomial distribution of heat flux	34
Figure 17 – Sequential activation of the control points: a) when $y_4 \geq y_2$ and b) when $y_3 \leq y_4 > y_2 > 0$	35
Figure 18 – Hybrid distribution of heat flux	36
Figure 19 – Experimental temperature in point T1	37
Figure 20 – Temperatures experimentally measured	38
Figure 21 – Temperatures experimentally measured	39
Figure 22 – Torque experimentally measured	40
Figure 23 – Experimental and numerical temperatures using the concentrated dis- tribution	41
Figure 24 – Experimental and numerical temperatures using the concentrated dis- tribution	42
Figure 25 – Error variation along the optimization process	43
Figure 26 – Numerical and experimental temperature in all thermocouples using linear distribution	44
Figure 27 – Experimental and numerical temperatures using the linear distribution	45
Figure 28 – Error variation along the optimization process	46
Figure 29 – Heat flux in the polynomial distribution	47
Figure 30 – Numerical and experimental temperature in all thermocouples using polynomial distribution	48

Figure 31 – Experimental and numerical temperatures using the polynomial distribution	49
Figure 32 – Error variation along the optimization process	50
Figure 33 – Polynomial fraction of heat flux in the hybrid distribution	51
Figure 34 – Numerical and experimental temperature in all input points using hybrid distribution	52
Figure 35 – Experimental and numerical temperatures using the polynomial distribution	53
Figure 36 – Initial temperature variation in each distribution	55
Figure 37 – Workpiece temperature distribution to different heat flux distributions	57
Figure 38 – Experimental and numerical temperatures in T1	58
Figure 39 – Experimental and numerical temperatures in T1	59
Figure 40 – Experimental and numerical temperatures in T3	60
Figure 41 – Experimental and numerical temperatures in T3	61
Figure 42 – Experimental and numerical temperatures in T5	62
Figure 43 – Experimental and numerical temperatures in T5	63
Figure 44 – Influence of element size in the maximum temperature variation simulated	69
Figure 45 – Influence of drilling step time in the maximum temperature variation simulated	70
Figure 46 – Influence of cooling step time in the maximum temperature variation simulated	70

List of Tables

Table 1 – Distribution of the cutting energy	8
Table 2 – Material Properties	21
Table 3 – Temperature points used in inverse procedure	25
Table 4 – PSO parameters used in the inverse procedure	26
Table 5 – Reaction times for experimental temperatures	39
Table 6 – Maximum measured temperature variations	39
Table 7 – Average error at each temperature using concentrated distribution . . .	41
Table 8 – Average error at each temperature using linear distribution	43
Table 9 – Polynomial Coefficients	45
Table 10 – Average error at each temperature using polynomial distribution	47
Table 11 – Hybrid coefficients	50
Table 12 – Average error at each temperature using hybrid distribution	51
Table 13 – Average error to each heat flux distributions	53
Table 14 – Heat flux transferred to workpiece	54
Table 15 – Average error in T1 to each heat flux distributions	58
Table 16 – Reaction times for temperatures in T1	59
Table 17 – Maximum temperature variations in T1	59
Table 18 – Average error in T3 to each heat flux distribution	60
Table 19 – Reaction times for temperatures in T3	60
Table 20 – Maximum temperature variations in T3	61
Table 21 – Average error in T5 to each heat flux distribution	62
Table 22 – Reaction times for temperatures in T5	62
Table 23 – Maximum temperature variations in T5	63

List of Symbols

Abbreviations

FEA Finite Element Analysis

FEM Finite Element Model

IHCM Inverse Heat Conduction Method

IHCP Inverse Heat Conduction Problem

PSO Particle Swarm Optimization

RMSE Root mean squared error

Greek Symbols

ΔT Temperature variation

δT Arbitrary variational field

$\Delta_{t,c}$ Step time of cooling phase

$\Delta_{t,d}$ Step time of drilling phase

ω Inertia weight

ϕ_g Social constant factor

ϕ_p Cognitive constant factor

ρ Material density

Nomenclatures

\dot{E}_{gen} Energy generated

\dot{E}_{in} Energy that enters a control volume

\dot{E}_{out} Energy that out a control volume

\dot{E}_{stor} Energy storated

\dot{U} Internal Energy

a Length of the uniform portion of the linear distribution

$c_0, c_{11}, c_{12}, c_{21}, c_{22}, c_{31}, c_{32}$ Coefficients of polynomial distribution of heat flux

C_p	Specific heat capacity
D	Number of dimensions of the inverse problem
d_1	Drill diameter
D_h	Hole diameter
D_w	Workpiece diameter
E_1, E_2, E_3, E_4	Element sizes
err_{abs}	Absolute error
err_{av}	Average error
err_{max}	Maximum error
f	Feed rate
F_c	Cutting force
g	The best particle among all the particles in the population
h	Convective heat transfer coefficient
I	Number of input points
k	Thermal conductivity
l_1	Drill length
l_2	Thread length
L_h	Hole length
L_w	Workpiece length
M	Measured drilling torque
N	Number of temperature points at each input point
n	Rotation speed of the drill
P_i	Vector of the best previous positions
p_{iD}	The best previous position of a particle
Q_1, Q_2, Q_3, Q_4	Control points of polynomial distribution of the heat flux
Q_r	Heat flux in the direction r

Q_z	Heat flux in the direction z
Q_{conv}	Convective heat flux
Q_{max}	Maximum heat flux in the linear distribution
Q_{total}	Total heat generated on machining
Q_{wp1}	Heat flux in the primary heat zone
Q_{wp2}	Heat flux in the secondary heat zone
Q_{wp}	Heat flux to workpiece
r_g	Social random factor
r_p	Cognitive random factor
S	Swarm size
t_2	Time to activate the control points Q_1 ad Q_2
t_3	Time to activate the control point Q_3
T_{in_exp}	Experimental temperature at input point i and temperature entry point n
T_{in_num}	Numerical temperature at input point i and temperature entry point n
t_{sim}	Simulation time
t_{T1_exp}	Time of variation of one degree at thermocouple T1
v_c	Cutting velocity
V_i	Vector of the particles' velocity
v_{iD}	Particle's velocity at one dimension
X_i	Vector of the particles' position
x_{iD}	Particle's position at one dimension
y	Distance from the drill cutting edge to the top surface of workpiece
y_1	Position of control point Q_1
y_2	Position of control point Q_2
y_3	Position of control point Q_3
y_4	Position of control point Q_4

Contents

1	INTRODUCTION	1
1.1	Objectives	2
1.2	Dissertation Structure	3
2	LITERATURE SURVEY	5
2.1	Drilling Process	5
2.2	Temperature influence on wet and dry machining	6
2.3	Identification of temperature distribution on machining process . . .	8
2.3.1	Moving heat source method	9
2.3.2	Finite difference method	10
2.3.3	Semianalytical methods	10
2.3.4	Finite Element Methods	11
2.4	Finite Element Methods in Drilling Process	12
2.4.1	Advection Model	12
2.4.2	Surface Heat Model	14
2.4.3	Heat Carrier Model	14
2.4.4	Ring Heat Model	15
2.5	Temperature Measurement	15
2.6	Inverse Heat Transfer Problem	16
2.7	Particle Swarm Optimization	17
3	MATERIALS AND METHODS	21
3.1	Materials	21
3.2	Methods	24
3.3	Inverse Procedure	25
3.4	Analyzed parameters	26
4	NUMERICAL MODELING	27
4.1	Finite Element Model	27
4.2	Heat transfer analysis	27
4.2.1	Spatial discretization	30
4.2.2	Time integration	31
4.3	Heat Flux Models	32
4.3.1	Concentrated heat flux	33
4.3.2	Linear distribution	34
4.3.3	Polynomial distribution	34

4.3.4	Hybrid distribution	36
5	RESULTS	37
5.1	Experimental Results	37
5.2	Concentrated Distribution	40
5.3	Linear Distribution	42
5.4	Polynomial Distribution	45
5.5	Hybrid Distribution	49
5.6	Comparision between the distributions	53
5.6.1	Thermocouple T1	58
5.6.2	Thermocouple T3	59
5.6.3	Thermocouple T5	61
6	CONCLUSIONS	65
6.1	Suggestions for Future Works	66
A	MESH REFINIMENT	69
	BIBLIOGRAPHY	73

1 Introduction

Drilling is one of the most applied processes in the industry, despite being one of the most complex processes. Much of this complexity is due to the geometry of the tool. The enclosure of the tool tip during machining is one of the main factors generating thermal problems. The thermal exchange capacity of the cutting region of the tool is limited considerably by this enclosure because of the larger the hole depth the greater the difficulty in dissipating heat. This generates increasingly higher temperatures in the tool-chip interface and in the workpiece. This consequently reduces tool life, generates geometric distortions in the workpiece and process errors.

In the primary and secondary shear zones, there is heat generation due to the plastic deformation of the workpiece material. This is one of the temperature sources that is transferred to the workpiece, tool, and chip. Heat is also generated along the tool-chip interface due to friction (TAY, 1993). The cutting fluid is commonly employed to try to lower the temperature in the process. The main purpose of the fluid is to lubricate, remove the chip and cool the cutting tool.

One of the problems of using cutting fluid is the high cost involved. According to Weinert et al. (2004) at around 17 % of the cost of machining is due to the use of cutting fluid. The total cost is due to both the cost of the use itself and the cost of disposal of the fluid used (BARADIE, 1996). The cutting fluid is very harmful to the environment, so the disposal of the products is critical in the industry (SOKOVIĆ; MIJANOVIĆ, 2001). This environmental concern and also with sustainability has increased considerably in recent years. For these reasons, the reduction and even the complete elimination of the cutting fluids are desired sometimes.

The elimination of cutting fluid in the drilling process makes the temperature critical and can cause problems in the production. The prediction of heat flux into chip, workpiece, and tool is difficult. This is calculated through the measurement of temperature in different locations of the workpiece.

The measurement of the temperature in the workpiece has been developed, although it is still very difficult to use only the information available in the literature because small differences in the process parameters are capable of generating great uncertainties (DAVIES et al., 2007). Due to the difficulty of obtaining conclusive results with purely experimental methods, several numerical methods have been used to determine the temperature distribution during the process. Among the various methods used one of the approaches is the finite element method.

The combination of the experimental temperature measurement with the finite element method allows the application of an inverse method of minimizing the error between experimental and numerical results to identify the heat flow that is transferred to the workpiece during drilling.

Different approaches can be used to determine the heat flux. Among these approaches, the Particle Swarm Optimization (PSO) is becoming popular due to the easy application and good efficiency in inverse problems.

The drilling parameters from machining tests are used as input to the thermal simulations. Almost all energy in machining is converted into heat. The heat flows into the workpiece is usually considered as constant along the process. The problem in the simulation of the drilling process is to determine the heat flow distribution on the wall of the hole, which can significantly influence the temperature distribution in the workpiece.

Regarding the temperature distribution estimation in the drilling of a complex workpiece, the simulation is carried out considering a heat flux distribution moving along the elementary hole's wall.

This work deals with the calibration of three different heat flux distributions. Based on experimental results of embedded thermocouples in a sample, an inverse heat conduction method is applied in order to determine the best parameter values for each model. Finite element analysis of a simple workpiece with already preexisting boreholes is conducted in order to estimate the temperatures. An error function based on the difference between predicted and measured temperatures is minimized through Particle Swarm Optimization (PSO).

1.1 Objectives

The main objective of this work is to identify best heat flux distribution transferred to the workpiece using a finite element model that considers a preexisting hole.

Furthermore, as secondary objectives:

- Implementation of four different heat flux models during the drilling process using a finite element model developed in Abaqus.
- Development of an experimental setup to measure the temperature of a workpiece during the drilling.
- Implementation of an inverse procedure using PSO to optimize the parameters of heat flux models through the minimization of the error between measured and simulated temperatures.

1.2 Dissertation Structure

This work is divided into four chapters. The first chapter is the state of the art. The objective of this chapter is to present the current state of research related to the influence of temperature on drilling. We present different numerical methods that are used to calculate the temperature distribution and the heat flux associated with the process. In a more detailed way, some thermal models are presented within the finite element method that is used to simulate the drilling process. We also review some methods used in temperature measurement and the inverse heat problem that combines experimental measurement with the numerical method. Finally, it is reviewed the use of PSO as a tool for solving inverse problems.

In the second chapter, we present all the materials used to obtain the experimental data. The experimental procedure is also described. These experimental results are used in an inverse procedure that is presented at the end of this chapter.

The third chapter refers to the numerical model used in the work to identify the heat flux. It is presented the thermal model used, the finite element model that was developed in Abaqus and the heat distributions that were analyzed.

Finally, the results obtained for each of the proposed heat distributions are presented. These results are discussed in order to analyze the effectiveness of the proposed procedure and which of the heat distributions best represents the drilling process.

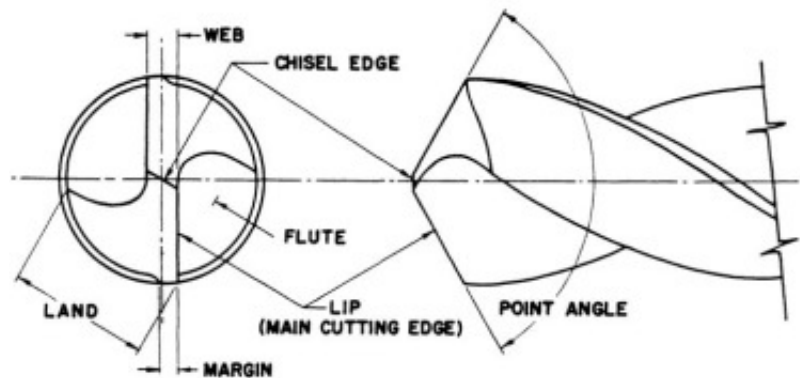
2 Literature Survey

2.1 Drilling Process

The drilling process is characterized by the rotational motion of the tool, while the table feeds toward the tool rotary axis. Due to the resulting movement, chips are formed at the drill edge and are transported out of the hole by the helical flutes of the drill.

Different drilling processes were developed in order to achieve different objectives, such as material removal rate, hole depth, dimensional accuracy and surface quality (KLOCKE, 2005). The spiral drill is one of the most important drilling tools for creating cylindrical drill holes from solid material or to enlarge the diameter of an existing hole (KLOCKE, 2005). The geometry of a spiral drill point is shown in the Figure 1.

Figure 1 – Geometry of a spiral drill point



Source: Klocke (2005)

The drill edge is formed by the main cutting edges and the chisel edge. The chisel edge has a highly negative rake angle and hence deforms the workpiece material plastically, forcing it to the main cutting edges (KLOCKE, 2005).

Other important drill parameters are (SHAW; COOKSON, 2005):

- helix angle
- point angle
- web thickness
- clearance angle
- drill diameter

Despite the importance of machining holes in a workpiece, the drilling process presents some particular drawbacks (KÖNIG; FERTIGUNGSVERFAHREN, 1990 apud ZEILMANN et al., 2003):

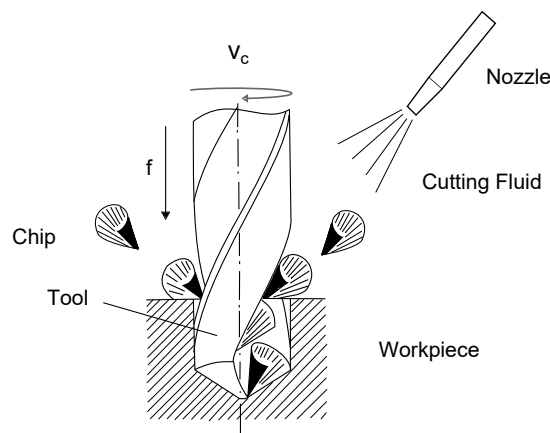
- the effective cutting speed reduces toward the center of the drill, reaching the value of feed rate in the tool axis;
- difficult in the chip removal;
- inadequate heat distribution in cutting zone;
- high tool wear when sharp edges are present;
- friction between the guides and the wall of the hole.

2.2 Temperature influence on wet and dry machining

The cutting fluids play a fundamental role in the drilling process. The main functions are to lubricate, cool and flush chip away from the cutting zone. Since the tool is constrained in a hole, the tool temperature tends to be higher than in other processes under similar conditions. The high temperatures at the tool tip have great influence on the tool life and workpiece surface quality (SATO et al., 2013).

The most common method of cutting fluid application is the flooding by means of a nozzle system. A great amount of cutting fluid is delivered directly on the tool and workpiece. Usually, there is no control of flow rate and volume. Furthermore, the counterflow of the chips inhibits the fluid to reach the drill tip, as Figure 2 exemplifies.

Figure 2 – Nozzle system



Source: Author's Production, 2017

The main function of cutting fluids is to reduce heat generated due to friction during cutting. This is performed in order to achieve better tool life, surface finish, and

dimensional tolerances. There is also used to prevent the formation of built-up edge and to facilitate the transportation of chips.

These problems associated with the wet machining, worsened by higher costs, health issues and contamination has contributed to the development of processes without cutting fluids. According to Soković and Mijanović (2001), which presented some ecological aspects of cutting fluids, the machine operators can be affected by contact with several substances. After the use, the disposal of the cutting fluids can be performed inside the company building or externally, usually at the waste disposal. If the cutting fluids are not properly discarded, ground, water and/or air pollution may occur.

Different approaches have been investigated on the last year, aiming to minimize or eliminate the cutting fluid application. The total elimination of cutting fluids would be a great advancing. However, some benefits of cutting fluids are not included in the dry machining and because of this tools. Without the cutting fluids, tools and workpieces are subjected to higher thermal loads.

Lauro et al. (2013) investigated the heat flow and the convective coefficient applying cooling systems at high-speed drilling of hardened steel. Flooded lubricant and the minimum quantity of lubricant (MQL) were compared with dry tests. FEM was applied to determine the heat flux and the convective coefficient for the cooling systems. In order to represent the effect of the tool motion (heat source movement), changes were performed on the heat generation and convective coefficients of the elements. They concluded that the heat flow into the workpiece and the convective coefficient were close to the literature reference.

Hussain et al. (2008) investigated the use of MQL in the deep hole drilling process. They studied the process in order to replace the usual method of drilling main oil gallery holes in aluminum alloy cylinder blocks. Good workpiece quality characteristics were obtained.

In drilling, when the cutting fluid is not supplied through the spindle, the tool tip suffers from high temperature, leading to rapid wear. In this case, the cooling of the drill tool body may contribute significantly, removing the heat generated at the tool-chip interface (PONTES, 2017).

As pointed out by Fleischer et al. (2007), the heat input caused by the lack of coolant may lead to workpiece thermal distortion. In dry machining, the heat generated is no longer removed by the cutting fluid. Therefore, the workpiece can distort due temperature changes on several regions of the workpiece. The workpiece distortion during the entire machining process can affect its dimensional accuracy.

In this regard, Aurich et al. (2014) optimized the cutting conditions in order to decrease the geometrical deviation. The machining accuracy was improved through experiments and finite element simulations of the dry turning of aluminum workpieces.

These analysis showed that higher cutting speeds decrease thermal loads of the workpiece.

Denkena et al. (2010) studied the surface errors generated by induced temperatures. This study was performed on thin-walled workpieces. Within the experimental investigation, the influences of thermal-induced deflections were separated from force-induced deviations. The results emphasized the dominance of the thermal deviations for the machining of the thin-walled workpiece.

2.3 Identification of temperature distribution on machining process

The heat generated on machining process was one of the first and most researched topics in machining. Taylor (1907) was a pioneer on the studies related to tool wear, he discovered that high temperatures of the tool were associated with reduced useful life. Also, he developed an empirical relationship between the cutting speed and tool life. Ber and Goldblatt (1989) also showed the influence of the temperature in tool's life, a large temperature gradient results in a smaller rate as well as low level of the tool wear.

Almost all the energy poured to the system is converted into heat. This energy flows into the tool, workpiece, and chip. Fleischer et al. (2007) presented a literary research of the cutting energy distribution comparing the drilling, turning and milling processes and it is presented at Table 1.

Table 1 – Distribution of the cutting energy

	Drilling	Turning	Milling
Tool	5 - 15 %	2,1 - 18 %	5,3 - 10 %
Workpiece	10 - 35 %	1,1 - 20 %	1,3 - 25 %
Chip	55 - 75 %	74,6 - 96,3 %	65 - 74,6 %

Source: Fleischer et al. (2007)

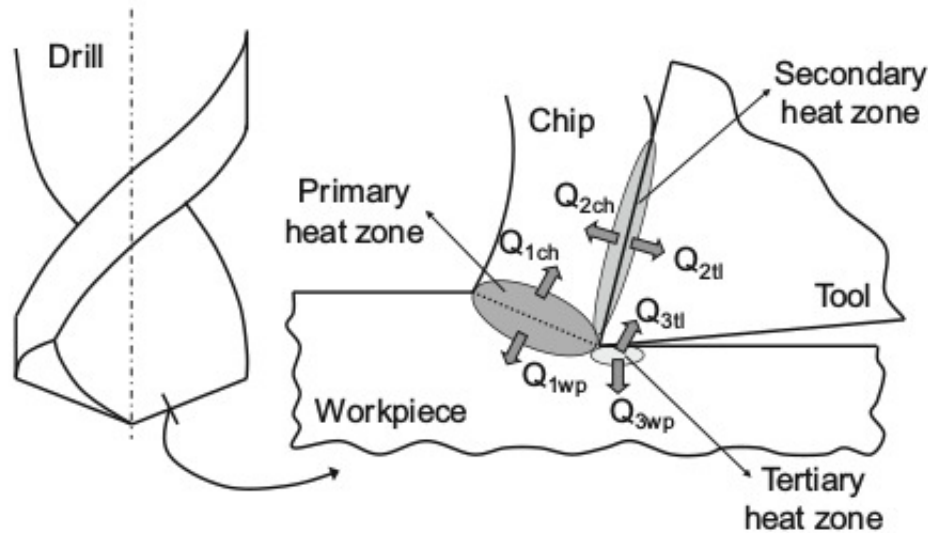
From Table 1, it can be seen that the heat flow into the workpiece fluctuates. In drilling, the input energy flowing to the workpiece during the process is estimated from 10 to 35 % of the overall cutting energy. As a result of this heat balance, the temperature fields formed in the workpiece and tool changes until the equilibrium between added and removed heat is achieved (KLOCKE, 2005).

The energy put into the process ($F_c \cdot v_c$) goes into friction and especially in shear, due to the deformation process. The plastic deformation occurs at the primary plane and the friction happens at the tool-chip interface. The heat generation occurs in a very small zone of the cutting tool. Thus, the cutting edge experiences high temperatures, strongly influencing tool wear, workpiece surface integrity, and the chip formation mechanism.

The Figure 3 shows a model of three different heat generation regions in the cutting zone. At the primary heat zone or shear zone, the heat is generated due to plastic

deformation of the workpiece material. At the secondary heat zone or tool-chip interface and tertiary heat zone or tool-workpiece interface, the heat is generated especially due to the friction between the bodies in contact. However, it is hard to determine the share percentage that is transferred to the tool, chip, and workpiece.

Figure 3 – Different heat-generation regions in the cutting zone



Source: Segurajauregui and Arrazola (2015)

The determination of the temperature distribution arising during cutting has long been the subject of intensive research. In this regard, Tay (1993) classified some methods used for calculating machining temperature as:

- the moving heat source method
- the finite difference method;
- semianalytical methods;
- the finite element method

2.3.1 Moving heat source method

Agapiou and DeVries (1990) presented a relatively simple method to determine the temperature distribution at the drill edges. Their approach can be used on steady-state and transient cases. They used the steady state temperature solution for a moving source by Jaeger (1942 apud TAY, 1993) and the transient solution for a constant heat flux on a surface.

Agapiou and Stephenson (1994) developed an analytical model to predict the transient and steady-state drill temperatures. Based on temperature solutions for a semi-infinite body and using a transient analysis to distribute heat between the drill, chip, and workpiece. Good agreement between calculated and measured values were found using this approach. This model was able to predict the partition of the heat flux which flows into the chip, the tool, and the workpiece.

Recently, models that use an analytical approach were proposed by Komanduri and Hou (2000), Karpas and Özel (2006), Dogu et al. (2006), Ulutan et al. (2009) and Islam et al. (2016).

2.3.2 Finite difference method

Rapier (1954) used the finite difference method (FDM) to calculate the temperature distribution. He considered the workpiece, the tool and the chip as three different regions, which were connected to each other by the shear plane and the chip-tool interface. He calculated the temperature distributions in three steps: first using FDM, calculating the temperature distribution in the part. Then, analytically, the temperature distribution was calculated on the chip. Finally, he used the FDM again to determine the tool temperature. With the results found for some cases, he concluded that the temperature at the chip-tool interface was lower on the tool side than on the chip, confirming the tendency shown by other authors that most of the process energy is directed to the chip.

Chip, tool, and workpiece were considered as a single system by Dutt and Brewer (1965). They proposed an assumption that the amount of heat generated in the shear plane and the chip-tool interface was known. However, the heat flux at each interface was an incognita. Discretizing the energy equation for each region. A single system was considered, this was proposed in order to decrease the number of variables. They were able to calculate the temperature distribution and the amount of heat directed to each side of the interface.

2.3.3 Semianalytical methods

On semianalytical methods, some parameters of the machining process, such as the surface temperature of the chip and part, are obtained experimentally. Then these values are used in analytical models to calculate the temperature distribution throughout the process.

Boothroyd (1963) developed a model to determine the temperature distribution in the workpiece, chip, and tool during orthogonal metal cutting. The author used infrared photography to record the superficial temperature in the chip, tool, and workpiece. However, his measurement system was only able to work properly on temperature above 600°C .

Though, this temperature may change the material mechanical properties. He estimated the proportion of heat which flowed to the workpiece and comparing it to Weiner (1955 apud TAY, 1993) he found that his values were lower than experimental values. He further compared with the method proposed by Rapier (1954) and found that the Rapier's method overestimated the interfaces temperatures.

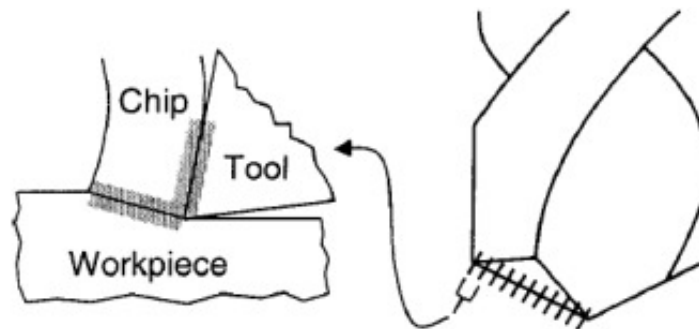
2.3.4 Finite Element Methods

In order to predict the workpiece, chip and tool temperatures, Finite Element Methods (FEM) have been successfully applied. Tay et al. (1974) was one of the first to use the finite element method to compute the temperature distribution in the tool, chip, and workpiece for orthogonal cutting process. Their approach consists on calculating the heat source distribution using the strain-rate and flow stress distributions. Flow stress was considered as a function of strain, strain-rate, and velocity. They were calculated from deformed grid patterns obtained from quick-stop experiments.

The authors were able to obtain an acceptable complete two-dimensional temperature distribution. Although the method was accurate to calculate the temperature distribution, the requirement of several experiments made the method a laborious process. The values obtained presented good agreement when compared to the experimental values of Boothroyd (1963). However, the requirement of some experimental data input for each machining condition, such as velocity and strain-rate, reduced the method viability.

Based on this method, there were developed simple models consisted on discretizing the cutting and chisel edges as fundamental elements, each element is then considered as a particular case of orthogonal cutting (Figure 4). Usually, to determine the amount of heat flowing into the tool, the heat flux loads consider both the heat generated on the shear plane and the heat generated on the tool rake face on each segment of the cutting edges (BONO; NI, 2006).

Figure 4 – The drill point and the orthogonal element model



Source: Bono and Ni (2006)

The temperature profile was analyzed along the cutting edges and the chisel edge

of a drill. Based on analytical equations, the heat flux loads were applied to the finite element model to simulate the temperature distribution in the drill. It was concluded that the maximum temperature can occur near the chisel edge and pointed out that the results predicted by the model were consistent with experimental observations.

Lazoglu et al. (2017) combines the analytical and FEM modeling to estimate the temperature of carbide tools in drilling of Ti-6Al-4V workpieces. They developed a special device to acquire the signal of a thermocouple attached to the rotating drill. There was a good agreement between the simulated and predicted temperatures.

2.4 Finite Element Methods in Drilling Process

To predict the temperature in the workpiece, few different thermal load strategies can be used. Chen et al. (2017) presented four different approaches to the heat flux distribution which are classified as:

- advection model;
- surface heat model;
- heat carrier model and
- ring heat model.

These thermal load strategies have been applied to simulate the temperature in drilling by several authors. These strategies focus on the workpiece temperature simulation which is one of the main subjects of this dissertation.

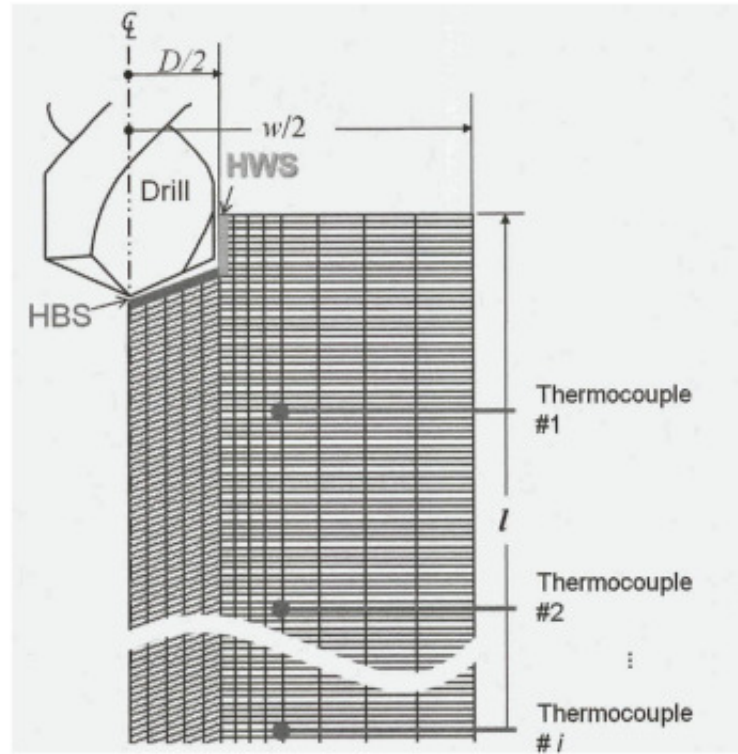
2.4.1 Advection Model

The advection model simulates heat transfer and material removal in two consecutive steps. The surface heat flux is loaded on the shear plane and the temperature distribution is calculated. After that, the element is removed at the end of each time step to simulate the chip removal.

In drilling process, the workpiece is usually discretized as shown in Figure 5, where the elements at the bottom of the hole are deleted as the tool feeds. This is performed in order to better represent the heat flux in the simulations.

Bono and Ni (2002) developed a model to predict the heat flow to the workpiece in dry drilling. The study used a two-dimensional, axisymmetric finite element model of the workpiece, created on Abaqus. As the drill moves into the workpiece, the heat flux is applied to the elements located directly beneath the cutting edge. The drill geometry and

Figure 5 – Workpiece finite element mesh



Source: Tai et al. (2012)

the measured drilling thrust and torque are used as inputs to calculate the heat flux loads. This model only considers the heat flux generated on the chip formation zone.

Biermann et al. (2012) simulated the heat loading into the tool and the workpiece in the deep hole drilling process, applying minimum quantity lubrication (MQL). They pointed out that the combination of the long machining time, internal working zone, and reduced cooling performance induces to high thermal load into the workpiece which may worsen the hole quality. A two-dimensional model of the workpiece was developed to simulate the temperature during the deep hole drilling process. Using a Finite Element Analysis (FEA), the temperature field within the workpiece was predicted. The simulated temperature showed good agreement with the measured data for the thermocouple position near the borehole wall.

Kuzu et al. (2017) applied minimum quantity lubrication (MQL) in deep-hole drilling. They used Finite Element Method to simulate the temperature distribution in the workpiece and the influence of the MQL. The heat flux loads on the chisel, cutting lip and on the margin were determined using a linear and exponential models. The model was calibrated at measured temperature throughout an inverse procedure. Good results were obtained.

Biermann and Iovkov (2013) applied a relatively constant and uniform distributed heat flow at the borehole ground. Actually, the drilling process was discretized by the segmentation of the borehole. As the tool feeded into the hole, the thermal conductivity of the corresponding FE-elements was set to a near-zero value. Considering the thermal conduction solution, the segment is eliminated. The simulation was divided into two stages. The first represented the drilling process with a heat source, while the second showed the cooling phase, which is implemented by convective heat transfer. They concluded that the precision of the model depends on the geometry, the discretization of the drilling process and the time step.

2.4.2 Surface Heat Model

The surface heat model is a simple application of surface heat flux on the element surface. In this case, no material removal is considered and, hence, no element is eliminated. Therefore, heat partition needs to be taken into account in order to determine the right amount of heat flowing into the workpiece or into the tool.

Chen et al. (2017) used a model that was modified from the single nodal heat model, developed by Kakade and Chow (1993), applying the surface heat flux on the element surface. The heat partition ratio was determined experimentally using the inverse heat transfer method, minimizing the discrepancy between model prediction and experimental measurement.

2.4.3 Heat Carrier Model

The heat carrier model consists on considering the moving tool as an isothermal heat carrier, conducting a constant surface heat flux into the workpiece. No element need to be eliminated.

Tai et al. (2012) investigated the workpiece thermal distortion in deep hole drilling using twist drill tool. They used FEA to predict the temperature. The advection model was used but they also proposed a heat carrier model to transfer heat from drill to workpiece. The heat sources were applied on the drilling hole bottom and wall surfaces. An inverse procedure were applied to determine the time-dependent heat fluxes. They distinctly simulated the heat flux on both surfaces. The results showed that, as the drilling depth increases, the heat power on the whole wall surface becomes more significant.

Although the good results, there was a requirement of measuring the temperature very close to the machined wall, which can experimentally be hard. Furthermore, the combination of simulations to predict two heat fluxes separately can lead to high computational cost. In addition, they pointed out that 2-D axisymmetric FEA model is suitable for modeling the drilling of a single hole in an axisymmetric workpiece, while a 3-D model

is required for workpieces with complex geometry and multiple holes.

2.4.4 Ring Heat Model

In the ring heat model, the heat flux is concentrated on a ring-shaped band, which simulates the tool path of one revolution. The ring moves along the axial direction and the heat flux is applied to one layer of elements.

Macedo (2015) simulated the thermal distortion of automobile workpieces by applying a ring-type distribution model in already pre-existing boreholes. Using this approach there is no need to eliminate elements as the tool feeds into the workpiece.

Faverjon et al. (2015) investigated the ring-shaped moving heat flux. A linear heat flux density distribution model was proposed. It considered the friction influence caused by the drill margins on the freshly generated surface, the radiation of the hot chips, the conduction and friction between the chips and hole. They used the inversion method to calibrate the heat flux models, measuring the temperature in a sample with several embedded thermocouples. Therefore, although the shape of the curves of the measured and predicted temperatures were similar, their values were quite discrepant, which can lead to errors in simulations of a complex workpiece.

2.5 Temperature Measurement

The prediction of the heat that flows to the workpiece is a difficult task. This happens due to the need to measure the temperature in different regions of the workpiece. The temperature measurement at the tool edge is also extremely difficult. These measurements are used in heat distribution determination. This occurs because of some factors like the narrow shear band, chip obstacles, and the nature of the contact phenomena where the two bodies, tool and chip (ABUKHSHIM et al., 2006).

Generally, the techniques used to measure temperature in metal cutting are tool-work thermocouples, embedded thermocouples, radiation pyrometers, metallographic techniques and a method of using powders of constant melting point (ABUKHSHIM et al., 2006).

The embedded thermocouple technique requires the drilling of several holes where the thermocouples are inserted. These thermocouples must be attached close to the surface to be measured. Kitagawa et al. (1997) used this technique to study the effect of temperature on tool wear on high speed turning of Inconel 718 and milling of Ti-6Al-6V-2Sn alloy. Tungsten micro-thermocouples were incorporated into the tool. Temperatures of 1200 and 1100°C were reported for the ceramic tool-Inconel at 150m/min and carbide-Ti-6Al-6V-2Sn tool at 500m/min, respectively. Chen et al. (1997 apud ABUKHSHIM et al.,

2006) calculated the heat flowing to the rake face of the cutting tool by using an inverse heat transfer method (IHTM) . The method used the interior temperature variations measured from a thermocouple.

2.6 Inverse Heat Transfer Problem

Normally, the heat flux is determined through an IHTM based on the workpiece temperature measured. The temperature can be recorded using thermocouples and analyzed using finite element method. With the improvement of computer capability, inverse techniques have become a popular means of resolving heat transfer problems in the last decade.

Inverse problem consists in obtaining an optimal set of model parameters using experimental temperature measurements. Finite element is used to simulate the temperature of the workpiece, adjusting the model parameters in order to minimize the error between the simulated and measured temperatures. Basically, it becomes an optimization problem, where different techniques have been applied. In the last years, some heuristic methods of solution have been used for inverse problems, which were based on pure intuition than on mathematical formality (OZISIK, 2000).

The estimation of a heat flux distribution or of a temperature gradient using a measured temperature history inside a solid is called the inverse heat conduction problem (IHCP). This is usually unstable because the solutions and parameters are determined from indirect observable data which contain measurement errors. Several methods, including analytical and numerical approaches, were developed to handle the IHCP in one, two and three-dimensional domains.

The inverse problem is based on the minimization of the error between a measured and a calculated temperature. An inverse analytical approach was used by Battaglia et al. (2005) to estimate the temperature. They did stationary and linearity assumptions to break down the 3D problem in a 2D problem. Some of the methods commonly used are the least squares method (CUI et al., 2012), the conjugate gradient method (LU et al., 2012), the function specification method (BLANC et al., 1998), genetic algorithms (GOSSELIN et al., 2009) and neural networks (DENG; HWANG, 2006). Among the heuristic methods, the Particle Swarm Optimization (PSO) has been widely applied. This occurs because the global optimum can be obtained without a complex implementation.

The application of the PSO to solve the inverse heat conduction problem wasn't very much studied, maybe because it is a relatively new optimizer. The effectiveness and efficiency of PSO in IHCP were studied by Vakili and Gadala (2009). Three variations of PSO were used to solve boundary IHCP in one, two and three dimensions, in steady and transient problems. The results showed that PSO can be successfully applied with a good

efficiency, when compared to a genetic algorithm, especially in more complex test cases.

It was also presented that the stability problem of the classical inverse approaches in dealing with smaller time steps, can be mitigated in PSO. Liu (2012) used PSO-based algorithms in the inverse analysis of surface heat flux for a three-dimensional heat conduction. He presented three different modifications in the PSO algorithm and some modifications resulted in performance improvement.

2.7 Particle Swarm Optimization

Evolutionary computation techniques work on a population of potential solutions on a search space. The PSO was designed and developed by Kennedy and Eberhart (1995) based on the social behavior theory. It was proposed a method for optimization of continuous nonlinear functions. A standard textbook that presents the social and computational paradigms of this method was written by Kennedy et al. (2001).

The PSO algorithm is initialized with a random potential solutions. Each one of these "solutions" is named as particle. Each particle is a point in a D -dimensional space, where D is the number of dimensions of each particle. The dimensions are the number of variables that are being optimized. The i th particle is represented as $X_i = (x_{1D}, x_{2D}, \dots, x_{iD})$ and these particles are manipulated according to the Equations 2.1 e 2.2.

$$v_{iD} = v_{iD} + \phi_p * r_p * (p_{iD} - x_{iD}) + \phi_g * r_g * (g - x_{iD}) \quad (2.1)$$

$$x_{iD} = x_{iD} + v_{iD} \quad (2.2)$$

where the best previous position is recorded and presented as $P_i = (p_{1D}, p_{2D}, \dots, p_{iD})$. The best particle among all the particles in the population is represented by the symbol g . The velocity (position change) rate for particle i is represented as $V_i = (v_{1D}, v_{2D}, \dots, v_{iD})$. ϕ_p and ϕ_g are two constants and r_p and r_g are two random functions in the range $[0,1]$.

Using the Equation 2.1 is calculated a new velocity to the particles. In the calculation, the previous velocity and the distances of particle current position from its own best position and the group's best position. Then the particle is moved to a new position, according to Equation 2.2. Each particle performance is measured using a predefined fitness function, which is related to the problem to be solved.

The second and the third parts of the velocity Equation 2.1 have the objective to change the velocity particle. Without these two parts, the particles would keep in the same

direction at the current speed until hit the boundary. The second part is the cognitive part, which represents the particle own history. The third part is the social part, which represents the collective history of the swarm when searching the best location. If ϕ_p is equal to ϕ_g , then the particle will search equally with cognitive and social parts. However, when one of the constants is bigger than other, the particle will use more of the related history (LI; QU, 2012).

A new version of particle swarm optimation was developed after the addition of a new inertia weight. The inertia weight ω is brought into the Equation 2.1 that is transformed in the Equation 2.3. This term plays the role of balancing the global search and the local search. It can be a positive constant or even a positive linear or nonlinear function of time (SHI; EBERHART, 1998). A large inertia weight facilitates the global search, while a small inertia weight facilitates the local search.

$$v_{iD} = \omega * v_{iD} + \phi_p * r_p * (p_{iD} - x_{iD}) + \phi_g * r_g * (g - x_{iD}) \quad (2.3)$$

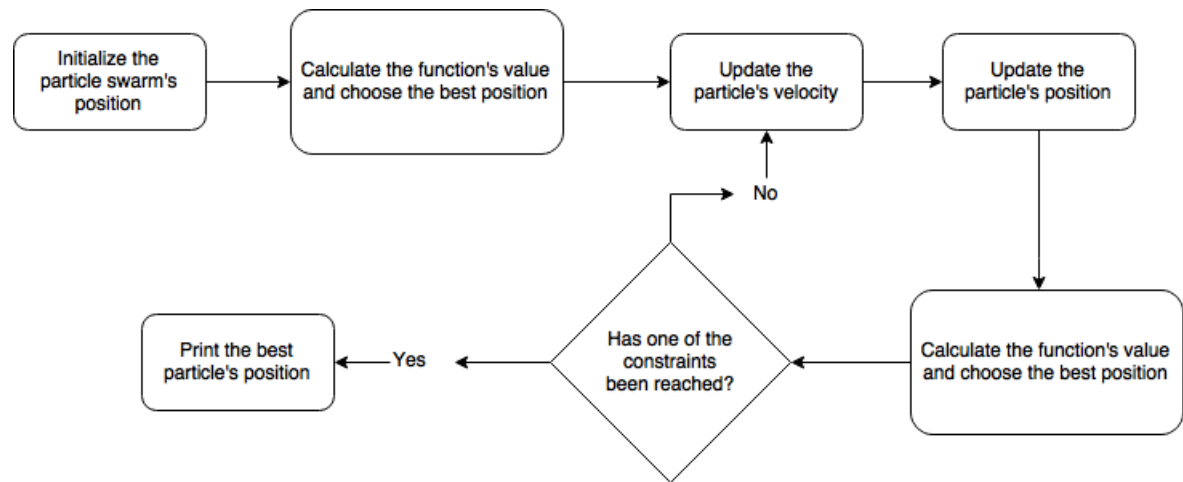
One of the parameters of the PSO is the number of particles (S), also called swarm or population. The influence of this parameter was studied by some researchers. Shi and Eberhart (1999) did an experimental study using the PSO and the results showed that its performance wasn't sensitive to the swarm size. The convergence analysis performed by Trelea (2003) demonstrated that in most of the cases, increasing the swarm size decreased the number of required algorithm iterations. The success rate was also increased significantly.

The PSO main objective PSO is to minimize an objective function that was predefined. Usually is an error function. The iterative process can be visualized in Figure 6. The iterative process is initialized with a swarm of S particles. The particle's positions are randomly generated and the value of x_{iD} is a number between 0 and 1. Each particle has a number D of dimensions, that is the number of variables that are being optimized. Each one of these variables has lower and upper bounds. When the particle has a position $x_{iD} = 0$, each variable will have the lower bound value. If a particle has position $x_{iD} = 1$, the variable will have the upper bound value.

The objective function's value to each particle is calculated and the particle position with the best result is stored. The particle velocity is then randomly calculated and updated. Then, a new swarm is randomly generated according to Equations 2.3 and 2.2. The objective function's value is calculated. If a better result is found, the respective particle position is stored.

The search for the best particle position is ended when one of the defined constraints are reached. The three constraints used are: the function's value change is less then a

Figure 6 – PSO diagram



Source: Author's production, 2017

predefined value. The position change is less than a predefined value. The maximum number of iterations without finding a better function's value is reached.

3 Materials and Methods

The experimental procedure adopted in the present work consists of drilling a cylinder and obtaining the temperature of the workpiece at some points during a determined time. In addition, the torque generated during the machining process was also recorded.

The objective of this is to show how the workpiece temperature measurements were carried out. These were then used in the inverse method to identify the heat flow. The torque value was also measured during the drilling process and used in the results discussion.

3.1 Materials

The material of the workpiece used in the present work was steel 1020 whose properties are presented in the Table 2. The sample used was a cylindrical part with a diameter of $D_w = 43 \text{ mm}$ and a length of $L_w = 60 \text{ mm}$.

Table 2 – Material Properties

Properties	Value
Density (kg/m^3)	7900
Specific Heat (KJ/kgK)	490
Conductivity (W/mK)	52

Source: Bergman and Incropera (2011)

The machining process was carried out in a machining center ROMI D600 with a maximum rotational speed of 10000 *rpm* which can be seen in Figure 7. The tool used to drill the workpiece was a HSS drill with TiN coating which is represented in Figure 8. The dimensions of the drill are $d_1 = 10.5 \text{ mm}$, $l_1 = 133 \text{ mm}$ and $l_2 = 87 \text{ mm}$.

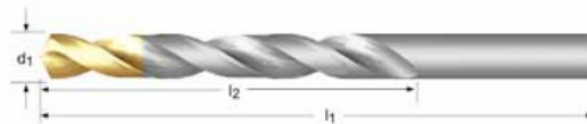
Using this tool a hole with depth of 50 *mm* was made in the center of the cylindrical part. The cutting speed used was $v_c = 40 \text{ m/min}$ and the feed rate was $f = 0.2 \text{ mm/rot}$. The drilling was performed without the use of cutting fluid due to the intention studyi the heat flow in dry drilling as a characteristic that becomes critical because of the lack of a refrigerant component.

Figure 7 – Machine tool used in research



Source: Author's production, 2017

Figure 8 – Tool used in research

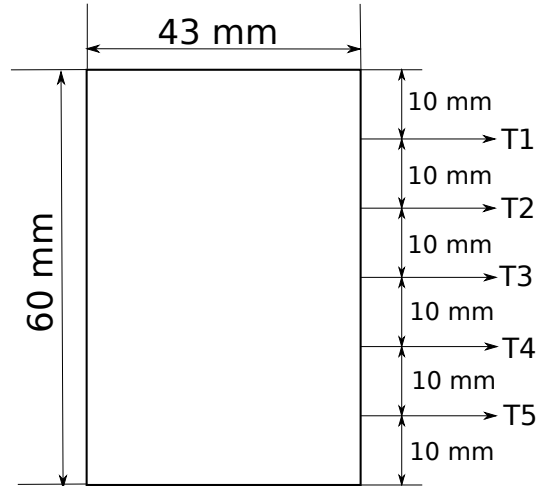


Source: Dormer (2015)

The workpiece temperature measurement was performed using five K-type thermocouples that were allocated throughout the part as shown in Figure 9. A 3mm diameter drill was used to drill five holes with 3mm depth and in each of these holes, a thermocouple was attached to the workpiece. These holes were filled with a high thermal conductivity paste to minimize the thermal resistance.

The thermocouples were connected to a National Instruments module which can be seen in Figure 10 and the measured temperatures were recorded with the aid of a program developed in Labview. The torque was measured during the machining process using a drilling dynamometer (Kistler 9272). The experimental setup can be seen in the Figure 11, the part was attached to the dynamometer and the thermocouples were fixed on it.

Figure 9 – Thermocouples' positions



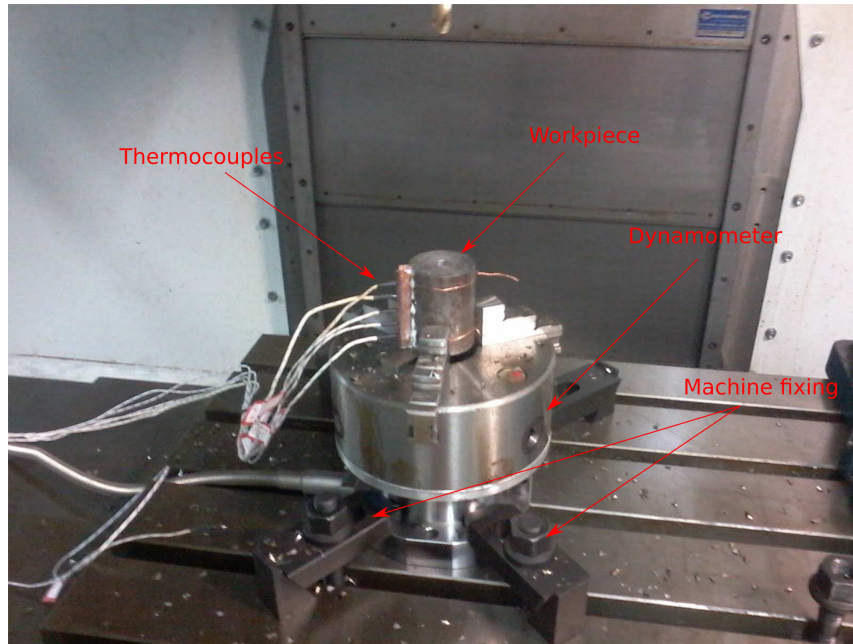
Source: Author's production, 2017

Figure 10 – National Instruments Module



Source: Author's production, 2017

Figure 11 – Experimental setup



Source: Author's production, 2017

3.2 Methods

The experimental procedures in many machining surveys are extremely complex, so in order to counteract the difficulties normally encountered in this area, a procedure that is as simple as possible was chosen. Some preliminary tests were performed to avoid electrical interference in measurements. The experimental apparatus was assembled in such a way that heat loss by conduction did not have a great impact on the study. After this initial care was taken, the experimental test that measured the desired parameters was actually performed.

The temperature of the workpiece in the five thermocouples were recorded for about 600 seconds. This time has been chosen so that the temperatures after the drilling could be stabilized. Although this uniformity cannot be fully guaranteed, it is possible to assume this because of the proximity of the measured temperatures.

After the results were obtained, it was decided to use the measured temperatures until the time $t_{sim} = 312.4 \text{ s}$ (12.4 s of drilling plus 300 s of cooling) which was enough for the thermocouples to reach a stability. The temperatures were recorded at a 100 Hz sampling rate.

The measured temperatures were then used in an inverse procedure to identify the heat flow that is transmitted to the part during the machining process. This procedure is described in the following section and seeks to determine the coefficients that define three

different types of distribution that are described in the section 4.3.

The torque measured by the dynamometer was recorded at a sampling rate of 1000 Hz . These measurements were used to determine the fourth heat flux by means of an analytical calculation whose result is presented to demonstrate the importance of the proposed inverse procedure and the efficiency of the proposed heat distribution models.

3.3 Inverse Procedure

The inverse procedure used in this study consisted in minimizing the mean error between the experimental and numerical results. The error function is defined by:

$$err_{proc} = \sum_{i=1}^I err_i / I \quad (3.1)$$

$$err_i = \sum_{n=1}^N \sqrt{\left[\frac{T_{in_exp}(t) - T_{in_num}(t)}{T_{in_exp}(t)} \right]^2} / N \quad (3.2)$$

where I is the number of thermocouples, T_{in_exp} and T_{in_num} are the measured and simulated temperatures at the point of entry and N is the number of temperature points at each input used in the error calculation. The points used in this analysis are presented in the Table 3. However, the number of temperature points varies according to each thermocouple. The 21 points showed in the table are used in T1, T2 uses the points 2 to 21, T3 uses 4 to 21, T4 uses 6 to 21 and T5 uses the points 8 to 21. There are differences in the number of points because the points with temperature variation less than 1 $^{\circ}C$ aren't used.

Table 3 – Temperature points used in inverse procedure

Point (n)	1	2	3	4	5	6	7
Time (s)	5.4	6.4	7.4	8.4	9.4	10.4	11.4
Point (n)	8	9	10	11	12	13	14
Time (s)	12.4	15.4	20.4	50.4	75.4	100.4	125.4
Point (n)	15	16	17	18	19	20	21
Time (s)	150.4	175.4	200.4	225.4	250.4	275.4	300.4

Source: Author's production, 2017

The inverse procedure in this study uses a PSO algorithm to determine the heat flow parameters of each distribution. The PSO was revised in the 2.7 section where the PSO parameters and their influence on the optimization process were presented. The parameters chosen in this study can be seen in the Table 4. The only parameter that

changes is the different analysis is the size of the swarm (S) related to the number of dimensions of each different distribution analyzed.

Table 4 – PSO parameters used in the inverse procedure

PSO Parameters	
Swarm size (S)	10 x D
Inertial weight (ω)	0.5
Cognitive factor (ϕ_g)	0.5
Social factor (ϕ_p)	0.5
Maximum number of iterations	10
The minimum position change	10^{-8}
The minimum objective value change	10^{-4}

Source: Author's production, 2017

According to Storn (1996), a swarm size of 10 x D for many applications is a good choice. The same author says that in the most of cases $\omega \in [0, 1]$, due to this it was chosen an intermediary value. The social and cognitive factors have the same value as the inertial weight so that the 3 factors have the same influence on the PSO. The maximum number of iterations is related to the computational capacity and it could be higher if better computers were used. The minimum objective value change is higher than the minimum position change to favor that this should be the stop criterion.

In the elaboration of the routine of the inverse procedure, was used the python language, all the PSO and the calculations of error were written in this language. The FEM was prepared in abaqus and recorded in a macro in python language.

3.4 Analyzed parameters

Some parameters of the temperature curves were analyzed in the results. The average error between measured and simulated temperatures. In the inverse procedure, just a few points were used. In the results analysis, points along all the measured time were used. The average error is calculated using point at each 1 s, the first point is like in the Table 3. In total, are used 308 points to T1, 307 to T2, 305 to T3, 303 to T4 and 301 to T5. The formulas used to calculate the average error are the same used to calculate the error in the inverse procedure (Equations 3.1 and 3.2).

Other important parameters of the temperature curves are the maximum temperatures with its respective times. It was also analyzed the reaction time that is defined as the necessary time to the temperature variation to reach one degree.

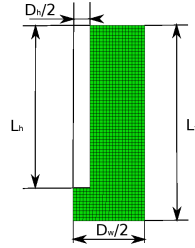
4 Numerical Modeling

Since the workpiece used in this work is a cylinder, the problem can be treated as a two-dimensional axisymmetric heat transfer model with coordinates in the radial(r) and axial(z) directions. The heat flux is applied as a moving heat source on the machined surface. The heat flux moves according to the feed.

4.1 Finite Element Model

The FEA of the workpiece temperature was performed using the commercial software ABAQUS 6.12. The Figure 12 shows the two-dimensional axisymmetric mesh used in this study. Workpiece and hole diameters are denoted as D_w and D_h . The workpiece length and the hole drilled are denoted as L_w and L_h . Four-node linear axisymmetric element (DCAX4) was selected in this study. The hole was considered already drilled and the heat source was applied to the hole wall through the subroutine *DFlux*.

Figure 12 – 2-D axisymmetric finite element mesh



Source: Author's production, 2017

This mesh type was chosen because of the geometrical conditions. The workpiece is a cylinder that can be represented by a rectangular section because the initial and load conditions are symmetric. The simulation was performed in two phases, the drilling phase, and the cooling phase. A mesh refinement was done to chose the characteristics as element size and step times to drilling and cooling phases. The values are element size $E = 1 \text{ mm}$, and step times $\Delta_{t,d} = 62 \text{ ms}$ and $\Delta_{t,c} = 1.0 \text{ s}$. The analysis that determined these values can be seen in the Appendix A.

4.2 Heat transfer analysis

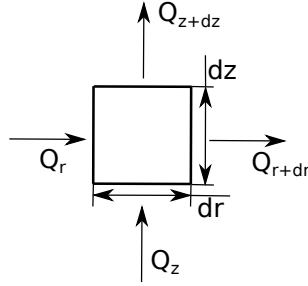
The problem solution is done by the commercial software Abaqus and it is important to understand how the thermal is solved. The assumptions that are done can be seen in Systemes (2013). In the software, it is assumed that the thermal and mechanical problems

are uncoupled in the sense that the rate of the internal energy depends only on the material temperature.

The heat balance of the workpiece comes from the first law of thermodynamics, which can be summarized as conservation of energy in Equation 4.1.

$$\dot{E}_{in} - \dot{E}_{out} + \dot{E}_{gen} = \dot{E}_{stor} \quad (4.1)$$

Figure 13 – Thermal problem



Source: Author's production, 2017

The Figure 13 represents the control volume to each element in the simulation. The heat balance is done for one element of the mesh. Considering the energy balance equation, the heat conduction entering in control volume is defined as Q_r and Q_z in the directions r and z . The control volume has dimensions of dr and dz . The heat entering is defined as:

$$\dot{E}_{in} = \dot{Q}_r + \dot{Q}_z = -kr dz \frac{\partial T}{\partial r} - kdr \frac{\partial T}{\partial z} \quad (4.2)$$

In this equation, k is the thermal conductivity of the workpiece material. The dz is the surface that is exposed to this heat conduction from direction r and dr is the surface relative to heat conduction in direction z . The heat conduction rates exiting the control volume from r and z directions can be found from Taylor series expansion. Derivating the heat conduction rates and ignoring higher order terms:

$$\dot{E}_{out} = \dot{Q}_{r+dr} + \dot{Q}_{z+dz} = \dot{Q}_r + \left(\frac{\partial \dot{Q}_r}{\partial r} \right) dr + \dot{Q}_z + \left(\frac{\partial \dot{Q}_z}{\partial z} \right) dz \quad (4.3)$$

There isn't heat generation in this problem, due this the therm \dot{E}_{gen} becomes zero. The amount of heat stored within the control volume is related to the density ρ , the specific heat capacity C_p and the rate of change in temperature, yielding:

$$\dot{E}_{stor} = \rho C_p \frac{\partial T}{\partial t} dr dz \quad (4.4)$$

As the maximum temperature measured isn't higher than 50 °C, then the thermal properties, thermal conductivity and specific heat, are considered constant with values: $k = 60.5 \text{ W/mK}$ and $C_p = 434 \text{ J/KgK}$. The radiation heat transfer is desconsidered in this analysis. The heat balance equation of the workpiece can be written as:

$$\dot{Q}_r + \dot{Q}_z - \dot{Q}_{r+dr} = \rho C_p \frac{\partial T}{\partial t} dr dz \quad (4.5)$$

The Equation 4.5 still can be simplified. The dimensional heat conduction rates become second derivates of temperature with corresponding dimension. The heat balance equation to the elements that are in the middle of the workpiece is:

$$\frac{1}{r} \frac{\partial}{\partial r} \left(kr \frac{\partial T}{\partial r} \right) dr dz + \frac{\partial}{\partial z} \left(k \frac{\partial T}{\partial z} \right) dr dz - \rho C_p \frac{\partial T}{\partial t} dr dz = 0 \quad (4.6)$$

Since the study is two-dimensional, and the system is considered to be stationary with air flowing around, there is heat loss by natural convection from the workpiece. This heat convection is included in the model as exiting the control volume to the surroundings, if the control volume in consideration has contact with surroundings. The convection heat is defined as:

$$\dot{Q}_{conv} = h dr dz (T - T_\infty) \quad (4.7)$$

where h is the convective coefficient between the workpiece and the ambient air flowing around. In the elements of the external surface that is in contact with the ambient air the Equation 4.6 becomes:

$$\frac{1}{r} \frac{\partial}{\partial r} \left(kr \frac{\partial T}{\partial r} \right) dr dz + \frac{\partial}{\partial z} \left(k \frac{\partial T}{\partial z} \right) dr dz - \rho C_p \frac{\partial T}{\partial t} dr dz = h dr dz (T - T_\infty) \quad (4.8)$$

To the elements that are in the drilling surface, the heat transferred to workpiece is entering the control volume. The Equation 4.6 becomes:

$$\frac{1}{r} \frac{\partial}{\partial r} \left(kr \frac{\partial T}{\partial r} \right) dr dz + \frac{\partial}{\partial z} \left(k \frac{\partial T}{\partial z} \right) dr dz - \rho C_p \frac{\partial T}{\partial t} dr dz = \dot{Q}_{wp}(t) dr dz \quad (4.9)$$

where $\dot{Q}_{wp}(t)$ is the heat transferred to workpiece during the drilling process.

4.2.1 Spatial discretization

A variational statement of the energy balance 4.6 is obtained by the standard Galerkin approach as:

$$\int \frac{1}{r} \frac{\partial \delta T}{\partial r} \left(kr \frac{\partial T}{\partial r} \right) dr dz + \int \frac{\partial \delta T}{\partial z} k \frac{\partial T}{\partial z} dr dz = \int \rho \delta T \dot{U} dr dz \quad (4.10)$$

where δT is an arbitrary variational field satisfying the essential boundary conditions.

The body is approximated geometrically with finite elements, then the temperature is interpolated as:

$$T = N^N(x)T^N, \quad N = 1, 2, \dots \quad (4.11)$$

where T^N are the nodal temperatures. The Galerkin approach assumes that δT , the variational field, is interpolated by the same functions:

$$\delta T = N^N \delta T^N \quad (4.12)$$

First and second order polynomials in one, two and three dimensions are used for the N^N . With these interpolations the Equation 4.10 becomes:

$$\delta T^N \left[\int \frac{1}{r} \frac{\partial N^N}{\partial r} \left(kr \frac{\partial T}{\partial r} \right) dr dz + \int \frac{\partial N^N}{\partial z} k \frac{\partial T}{\partial z} dr dz \right] = \int N^N \rho \dot{U} dr dz \quad (4.13)$$

and like the δT^N is arbitrarily chosen, it is found the equation:

$$\int \frac{1}{r} \frac{\partial N^N}{\partial r} \left(kr \frac{\partial T}{\partial r} \right) dr dz + \int \frac{\partial N^N}{\partial z} k \frac{\partial T}{\partial z} dr dz = \int N^N \rho \dot{U} dr dz \quad (4.14)$$

this is the time description of the geometric approximation of the elements that are in the middle of the workpiece. In the drilling surface and the external surface, we have respectively the Equations 4.15 and 4.16.

$$\begin{aligned} & \int \frac{1}{r} \frac{\partial N^N}{\partial r} \left(kr \frac{\partial T}{\partial r} \right) dr dz + \int \frac{\partial N^N}{\partial z} k \frac{\partial T}{\partial z} dr dz \\ & - \int h(N^N - T_\infty) dr dz = \int N^N \rho \dot{U} dr dz \end{aligned} \quad (4.15)$$

$$\int \frac{1}{r} \frac{\partial N^N}{\partial r} \left(kr \frac{\partial T}{\partial r} \right) dr dz + \int \frac{\partial N^N}{\partial z} k \frac{\partial T}{\partial z} dr dz + \int N^N \dot{Q} dr dz = \int N^N \rho \dot{U} dr dz \quad (4.16)$$

4.2.2 Time integration

Time integration in transient analysis is done using the backward difference algorithm:

$$\dot{U}_{t+\Delta t} = \frac{(U_{t+\Delta t} - U_t)}{\Delta t} \quad (4.17)$$

Introducing this term in the Equation 4.14 gives:

$$\begin{aligned} & \frac{1}{\Delta t} \int N^N \rho (U_{t+\Delta t} - U_t) dr dz - \int \frac{\delta T^N}{r} \frac{\partial N^N}{\partial r} \left(kr \frac{\partial T}{\partial r} \right) dr dz - \\ & \int \delta T^N \frac{\partial N^N}{\partial z} k \frac{\partial T}{\partial z} dr dz = 0 \end{aligned} \quad (4.18)$$

Like the Jacobian matrix to this system is not formed exactly, a modified Newton method is used to solve. The terms formation in the Jacobian matrix is described. The internal energy term gives a Jacobian contribution :

$$\frac{1}{\Delta t} \int_V N^N \rho \frac{dU}{dT} \big|_{t+\Delta t} N^M dr dz \quad (4.19)$$

Where $\frac{dU}{dT} \big|_{t+\Delta t}$ is the specific heat. The conductivity terms give a Jacobian contribution:

$$\int \frac{1}{r} \frac{\partial N^N}{\partial r} \left(k \big|_{t+\Delta t} r \frac{\partial N^M}{\partial r} \right) dr dz + \int \frac{1}{r} \frac{\partial N^N}{\partial r} \left(r \frac{\partial k}{\partial T} \big|_{t+\Delta t} \frac{\partial T}{\partial r} \big|_{t+\Delta t} \right) N^M dr dz \quad (4.20)$$

$$\int \frac{\partial N^N}{\partial z} k \big|_{t+\Delta t} \frac{\partial N^M}{\partial z} dr dz + \int \frac{\partial N^N}{\partial z} \frac{\partial k}{\partial T} \big|_{t+\Delta t} \frac{\partial T}{\partial z} \big|_{t+\Delta t} N^M dr dz \quad (4.21)$$

Including this terms in the Jacobian, the modified Newton to the elements in the middle of the mesh is:

$$\begin{aligned} & \left[\frac{1}{\Delta t} \int N^N \rho \frac{dU}{dT} \big|_{t+\Delta t} N^M dr dz + \int \frac{1}{r} \frac{\partial N^N}{\partial r} \left(k \big|_{t+\Delta t} r \frac{\partial N^M}{\partial r} \right) dr dz \right. \\ & + \int \frac{1}{r} \frac{\partial N^N}{\partial r} \left(r \frac{\partial k}{\partial T} \big|_{t+\Delta t} \frac{\partial T}{\partial r} \big|_{t+\Delta t} \right) N^M dr dz + \int \frac{\partial N^N}{\partial z} k \big|_{t+\Delta t} \frac{\partial N^M}{\partial z} dr dz \\ & + \left. \int \frac{\partial N^N}{\partial z} \frac{\partial k}{\partial T} \big|_{t+\Delta t} \frac{\partial T}{\partial z} \big|_{t+\Delta t} N^M dr dz \right] \bar{c}^{-M} = -\frac{1}{\Delta t} \int N^N \rho (U_{t+\Delta t} - U_t) dr dz \\ & - \int \frac{1}{r} \frac{\partial N^N}{\partial r} \left(kr \frac{\partial T}{\partial r} \right) dr dz - \int \frac{\partial N^N}{\partial z} k \frac{\partial T}{\partial z} dr dz \end{aligned} \quad (4.22)$$

with $T_{t+\Delta t, i+1}^N = T_{t+\Delta t, i}^N + \bar{c}^N$, $i = \text{iteration number}$

With the film condition, the convective flux term gives a Jacobian contribution:

$$\int N^N h N^M dr dz \quad (4.23)$$

adding this therm to the Equation 4.22, the modified Newton to the elements in the convective surface is:

$$\begin{aligned} & \left[\frac{1}{\Delta t} \int N^N \rho \frac{dU}{dT} \Big|_{t+\Delta t} N^M dr dz + \int \frac{1}{r} \frac{\partial N^N}{\partial r} \left(k \Big|_{t+\Delta t} r \frac{\partial N^M}{\partial r} \right) dr dz \right. \\ & + \int \frac{1}{r} \frac{\partial N^N}{\partial r} \left(r \frac{\partial k}{\partial T} \Big|_{t+\Delta t} \frac{\partial T}{\partial r} \Big|_{t+\Delta t} \right) N^M dr dz + \int \frac{\partial N^N}{\partial z} k \Big|_{t+\Delta t} \frac{\partial N^M}{\partial z} dr dz \\ & \left. + \int \frac{\partial N^N}{\partial z} \frac{\partial k}{\partial T} \Big|_{t+\Delta t} \frac{\partial T}{\partial z} \Big|_{t+\Delta t} N^M dr dz + \int N^N h N^M dr dz \right] c^{-M} \\ & = -\frac{1}{\Delta t} \int N^N \rho (U_{t+\Delta t} - U_t) dr dz - \int \frac{1}{r} \frac{\partial N^N}{\partial r} \left(k r \frac{\partial T}{\partial r} \right) dr dz \\ & - \int \frac{\partial N^N}{\partial z} k \frac{\partial T}{\partial z} dr dz \quad \text{with} \quad T_{t+\Delta t, i+1}^N = T_{t+\Delta t, i}^N + \bar{c}^N, \quad i = \text{iteration number} \end{aligned} \quad (4.24)$$

In the modified Newton to the elements in the drilling surface, it's added the therm relative to the heat flux transferred to the workpiece. The Equation 4.25 describes the time integration to these elements.

$$\begin{aligned} & \left[\frac{1}{\Delta t} \int N^N \rho \frac{dU}{dT} \Big|_{t+\Delta t} N^M dr dz + \int \frac{1}{r} \frac{\partial N^N}{\partial r} \left(k \Big|_{t+\Delta t} r \frac{\partial N^M}{\partial r} \right) dr dz \right. \\ & + \int \frac{1}{r} \frac{\partial N^N}{\partial r} \left(r \frac{\partial k}{\partial T} \Big|_{t+\Delta t} \frac{\partial T}{\partial r} \Big|_{t+\Delta t} \right) N^M dr dz + \int \frac{\partial N^N}{\partial z} k \Big|_{t+\Delta t} \frac{\partial N^M}{\partial z} dr dz \\ & \left. + \int \frac{\partial N^N}{\partial z} \frac{\partial k}{\partial T} \Big|_{t+\Delta t} \frac{\partial T}{\partial z} \Big|_{t+\Delta t} N^M dr dz \right] c^{-M} = \int N^N \dot{Q} dr dz \\ & - \frac{1}{\Delta t} \int N^N \rho (U_{t+\Delta t} - U_t) dr dz - \int \frac{1}{r} \frac{\partial N^N}{\partial r} \left(k r \frac{\partial T}{\partial r} \right) dr dz - \int \frac{\partial N^N}{\partial z} k \frac{\partial T}{\partial z} dr dz \\ & \text{with} \quad T_{t+\Delta t, i+1}^N = T_{t+\Delta t, i}^N + \bar{c}^N, \quad i = \text{iteration number} \end{aligned} \quad (4.25)$$

4.3 Heat Flux Models

The term \dot{Q}_{wp} in the Equation 4.9 is the fraction of heat generated in the process that is transferred to the workpiece. The heat flux in this research is considered as a spatial and time distribution along the hole wall. Four different heat flux models are used in this study concentrated, linear, polynomial and hybrid.

4.3.1 Concentrated heat flux

The concentrated distribution is calculated using an analytical approach. Assuming that all the energy in the cutting process is transformed into heat, the total heat can be calculated by the Equation 4.26:

$$Q_{total} = 2\pi M \frac{n}{60} t_c \quad (4.26)$$

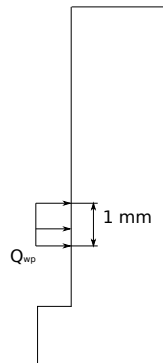
where M is the experimentally measured drilling torque, n is the rotation speed of the drill and t_c is the machining time. However, as previously presented, the heat input to workpiece (Q_{wp}) can occur in two of the three heat generation zones: the primary zone that is the tool bottom surface (Q_{wp1}) and the secondary zone that is the just-machined hole wall (Q_{wp2}), then just a portion of the heat generated is conducted to workpiece and it can be said that $Q_{wp} = Q_{wp1} + Q_{wp2}$.

As an input, simulation programs such as ABAQUS require a value independent of the simulation time Δt and the machined surface A , thus the heat quantity cannot be used. The quantity of heat transferred to workpiece ΔQ is put into relation to the surface machined within one second. The result thereof is referred to as the surface heat flux:

$$Q_{wp} = \frac{1}{A} \frac{\Delta Q}{\Delta t} \quad (4.27)$$

the calculated heat flux is put in the FEM of the workpiece, as can be seen in the Figure 14. The heat flux Q_{wp} is applied as a surface heat flux with uniform distribution in a size of 1 mm. This is the only flux that is not calculated through the inverse procedure.

Figure 14 – Concentrated distribution of heat flux

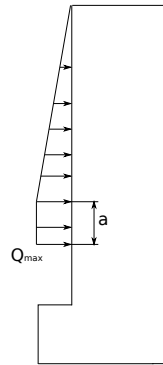


Source: Author's production, 2017

4.3.2 Linear distribution

The linear distribution is represented in Figure 15. The first part is an uniform distribution of length a and value Q_{max} . The second part is a linear distribution from Q_{max} until zero with length from a until the workpiece top surface. These two parameters a and Q_{max} are identified using the inverse procedure. This distribution was proposed by the author as a simple distribution. It considers the high heat input close to the cutting edge of the tool and the heat transfer along the machined surface.

Figure 15 – Linear distribution of heat flux

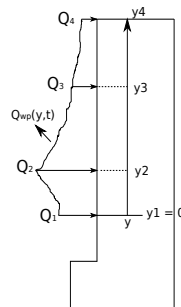


Source: Author's production, 2017

4.3.3 Polynomial distribution

The polynomial distribution is based in the approach presented by Tai et al. (2012). The spatial distribution of Q_{wp} at a specific time is defined as $Q_{wp}(y, t)$ where y is the distance from the drill cutting edge, as can be seen in Figure 16. The four control points used Q_1 , Q_2 , Q_3 and Q_4 and their positions y_1 , y_2 , y_3 and y_4 determine the spatial distribution of $Q_{wp}(y, t)$.

Figure 16 – Polynomial distribution of heat flux



Source: Tai et al. (2012)

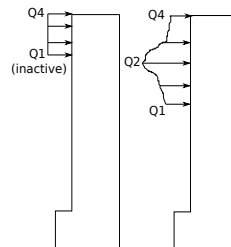
The heat generated in the primary heat zone usually is considered constant, but the heat flux in the hole wall increases as the hole depth increases. Because of this, the value of the control points varies in time and they are modeled as a quadratic function of time.

$$\begin{aligned}
Q_1 &= c_0 + c_{11} * (t - t_2) + c_{12} * (t - t_2)^2 \quad \text{for } t > t_2 \\
Q_2 &= c_0 + c_{21} * (t - t_2) + c_{22} * (t - t_2)^2 \quad \text{for } t > t_2 \\
Q_3 &= c_0 + c_{31} * (t - t_3) + c_{32} * (t - t_3)^2 \quad \text{for } t > t_3 \\
Q_4 &= c_0
\end{aligned} \tag{4.28}$$

where c_0 is the initially uniform distributed Q_{wp} . Time t_2 and t_3 are respectively the times to the drill reaches the depths y_2 and y_3 . The control point Q_1 moves according to cutting conditions (V_c and f) and the function of $Q_{wp}(y, t)$ is the polinomial interpolation of the control points.

The position of Q_4 is the only that varies in time, the other three points are fixed as $y_1 = 0$, $y_2 = 15mm$ and $y_3 = 30mm$. These values were chosen as suggested by Tai et al. (2013). The variation of the flux distribution has three stages. At the first stage, when $y_4 \geq y_2 > 0$, only Q_4 is active and the flux has a uniform distribution. The second stage starts at the moment that the drill reaches a hole depth greater than the value of y_2 , when $y_3 \leq y_4 > y_2 > 0$, and the control points Q_1 and Q_2 are activated. In the last stage, when $y_4 > y_3$, the control point Q_3 is activated. The times t_2 and t_3 are the necessary times to the tool reaches the depths y_2 and y_3 . In this drilling process $t_2 = 3.7 s$ and $t_3 = 7.4 s$. A sequential activation of the control points can be seen in the Figure 17.

Figure 17 – Sequential activation of the control points: a) when $y_4 \geq y_2$ and b) when $y_3 \leq y_4 > y_2 > 0$



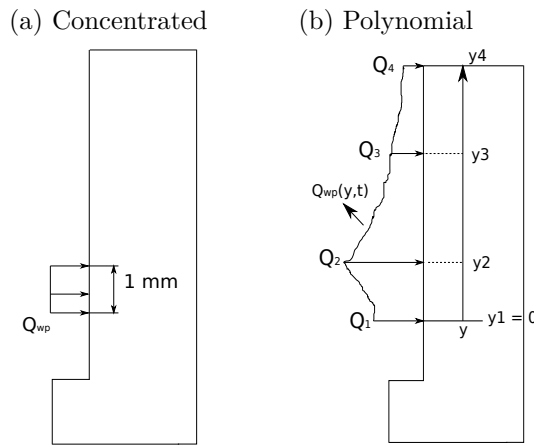
Source: Tai et al. (2012)

In the inverse procedure, the seven coefficients, $c_0, c_{11}, c_{12}, c_{21}, c_{22}, c_{31}$ and c_{32} , that define the control points are identified using the PSO to minimize the error between measured and simulated temperatures.

4.3.4 Hybrid distribution

The last distribution is similar to the polynomial distribution that was previously presented and it is called hybrid distribution. The difference is the addition of a concentrated heat flux of 1 *mm* length that moves together with control point Q_1 . This addition was done to analyze the influence of the high heat input in the primary heat zone. The heat flux distribution is presented in the Figure 18. The combination of these two heat fluxes is the hybrid distribution.

Figure 18 – Hybrid distribution of heat flux



Source: Author's production, 2017

This is a distribution proposed in this work. The eight coefficients are identified through the inverse procedure. The seven coefficients that define the polynomial flux more the coefficient Q_0 .

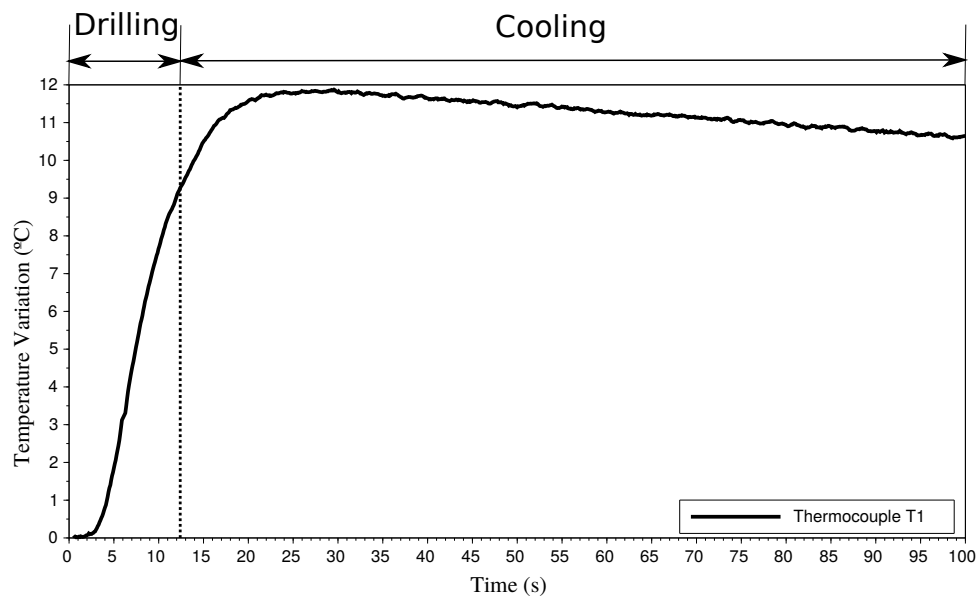
5 Results

At this chapter are presented the results found in the analysis. The chapter is divided in six sections. In the first section are discussed the experimental results. In the second section are presented the results to the concentrated flux. The third section presents the linear distribution and the polynomial distribution is in the fourth section. The last distribution, the hybrid distribution, is presented in the fifth section. In the sixth and last section are presented some comparisons between the proposed distributions.

5.1 Experimental Results

Looking specifically at one of the curves it can be seen the behavior of the temperature variation in the workpiece. The Figure 19 shows the temperature variation of thermocouple T1. A characteristic that is analyzed is the reaction time. The time necessary for the temperature variation to reach 1 °C.

Figure 19 – Experimental temperature in point T1



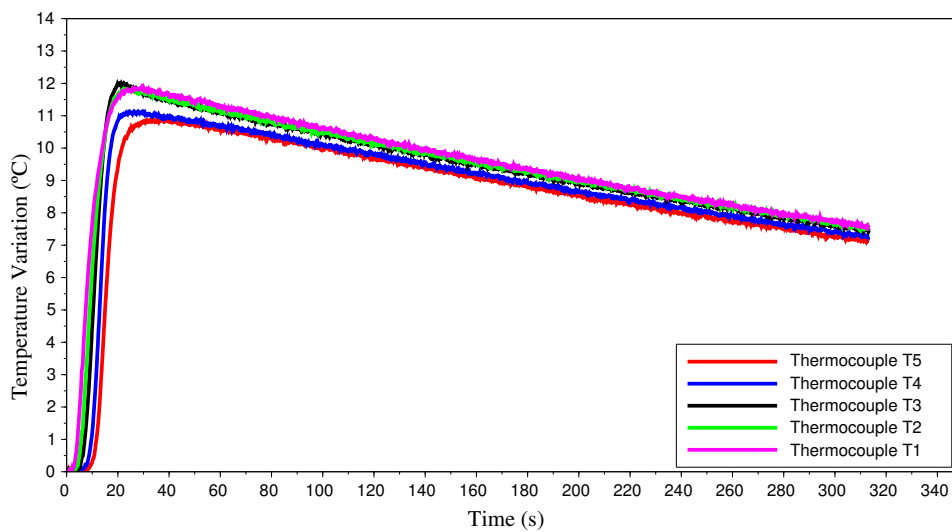
Source: Author's production, 2017

The temperature curve can be divided in two phases. The first is the drilling, where the machining process takes place and therefore a portion of the generated heat is transferred to the workpiece. The second phase is the cooling, where there is only heat transfer by convection and the homogenization of the workpiece temperature.

However, after the drill comes out of the hole the temperature of the points analyzed continue to increase. This occurs because the thermocouple localization is far from the machining surface. This is valid for the experimental and numerical analysis. After reaching the maximum temperature variation, (11.8°C) the temperature decreases linearly. This decrease in temperature happens due to the heat loss by convection, the heat transfer to other regions of the workpiece and the heat transferred to the fixture.

The experimental temperature curves are obtained as described in section 3.2. The results were plotted on time as can be seen in Figure 20. All curves have a similar behavior, your maximum values are located after the end of the drilling process. Up to the end of the analysis, the thermocouple temperatures have a temperature difference due to the thermocouple error. However, it can be considered that after 80 seconds the temperature in the five points of the workpiece is the same, since the difference is of 0.8°C and remains the same until the end.

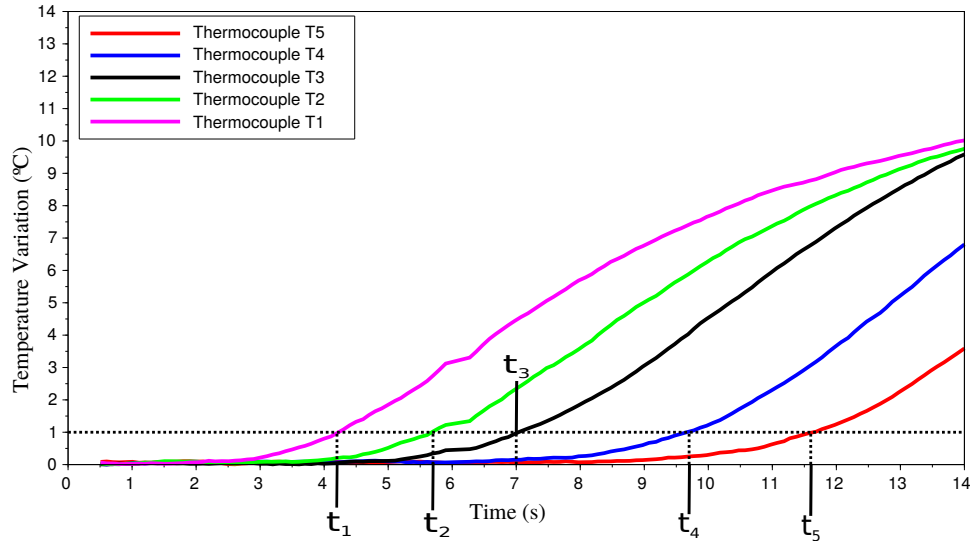
Figure 20 – Temperatures experimentally measured



Source: Author's production, 2017

Looking at the Figure 21, it can be seen that the behavior of the measured temperatures at the process beginning. The variation appears according to the position of the thermocouples attached to the workpiece. T1 is closest to the top of the workpiece and T5 in the bottom position. The Figure 21 and the Table 5 present the reactions time. It can be seen that they have the expected behavior.

Figure 21 – Temperatures experimentally measured



Source: Author's production, 2017

Table 5 – Reaction times for experimental temperatures

Thermocouple	T1	T2	T3	T4	T5
Reaction time (s)	4.2	5.7	7.0	9.7	11.6

Source: Author's production, 2017

The maximum temperature variations of each thermocouple are shown in Table 6. They are around $11.5^{\circ}C$. The thermocouples from T1 until T4 have their maximum values around the time of 20.4 and the thermocouple T5 has his maximum delayed in comparison with the other thermocouples.

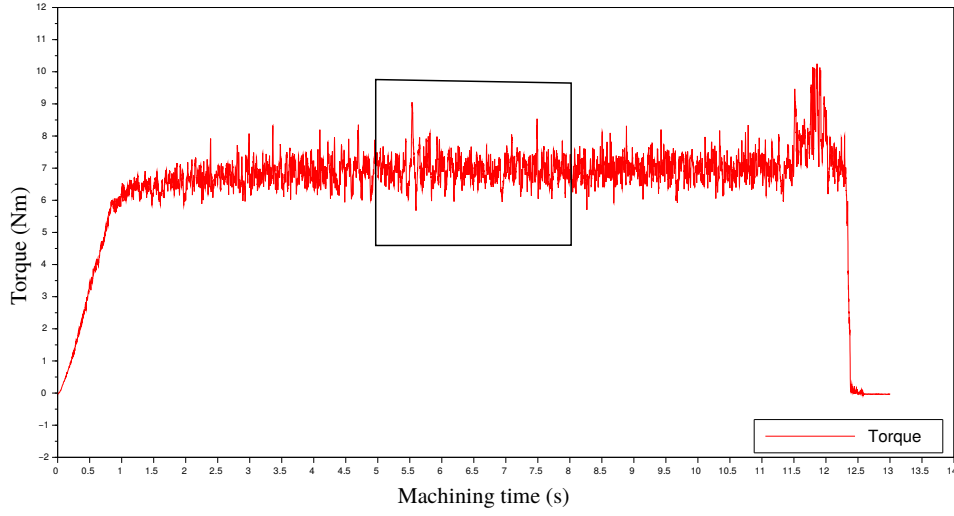
Table 6 – Maximum measured temperature variations

Thermocouple	T1	T2	T3	T4	T5
Maximum temperature variation ($^{\circ}C$)	11.9	11.8	12.0	11.1	10.9
Instant of time (s)	20.4	18.4	20.4	24.4	34.4

Source: Author's production, 2017

The torque was measured during the drilling process and its value was plotted on time, result presented in the Figure 22. The medium value of the torque is $M = 7.1 Nm$, it was calculated using the values in a period that is represented by the window in the figure. The torque is used to calculate the total heat generated in the drilling process.

Figure 22 – Torque experimentally measured



Source: Author's production, 2017

5.2 Concentrated Distribution

In the first analysis, it was considered a heat flux with a concentrated distribution as it was described in the section 4.3.1. The first step is to calculate the total heat generated using the Equation 4.26 as is shown in sequence.

$$M = 7.1 \text{ Nm}$$

$$n = 1212 \text{ rpm}$$

$$t_c = 12.4 \text{ s}$$

$$Q_{total} = 2\pi M \frac{n}{60} t_c = 11174 \text{ J}$$

However, only a portion of this generated heat is transferred to workpiece. The heat flux that is applied in the finite element model is calculated using the Equation 4.27. It was considered that 30 % of the generated flows into workpiece. The time of simulation is $dt = 12.4 \text{ s}$, then we have:

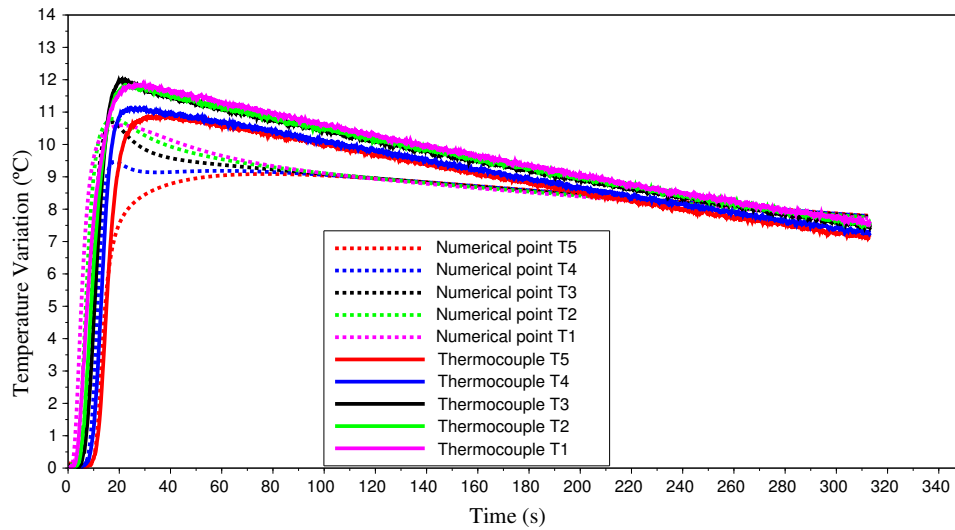
$$\Delta Q = 0.3 Q_{tot} = 3352.2 \text{ J}$$

$$A = 8.66 \times 10^{-5} \text{ m}^2$$

$$Q_{wp} = \frac{1}{A} \frac{\Delta Q}{\Delta t} = 3.12 \text{ MW/m}^2$$

With the heat flux calculated it's possible to calculate the numerical temperatures to all thermocouple positions. The comparison between the temperature variation obtained from numerical simulation and experimental results is presented in the Figure 23. This analysis has an average error of $err_{av} = 13.85 \%$. In the numerical curves, it can be observed that after 100 s the temperature tends to the same value. The experimental values show a bigger difference. This difference in the measured temperatures is a consequence of the thermocouples errors.

Figure 23 – Experimental and numerical temperatures using the concentrated distribution



Source: Author's production, 2017

The error to each temperature curve is different and this is presented in the Table 7. The best result found is to thermocouple T1 and the worst is T5. All results presented errors that are higher than 10 %. In the Figure 24, the temperature curves are plotted separately and it's possible to observe the differences between numerical and measured temperatures. In any of the temperatures, the maximum temperature variation of the experimental result is reached by the numerical value.

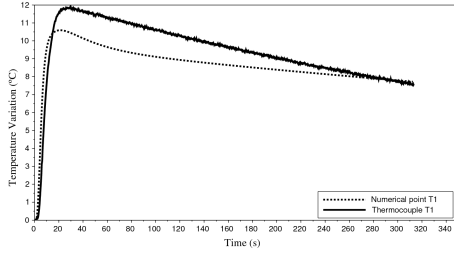
Table 7 – Average error at each temperature using concentrated distribution

Temperature	T1	T2	T3	T4	T5
Average error (%)	10.24	12.71	11.8	16.06	18.46

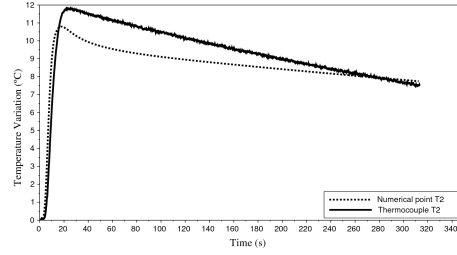
Source: Author's production, 2017

Figure 24 – Experimental and numerical temperatures using the concentrated distribution

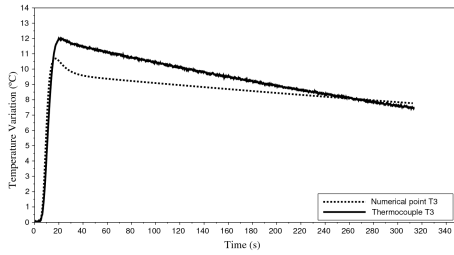
(a) T1



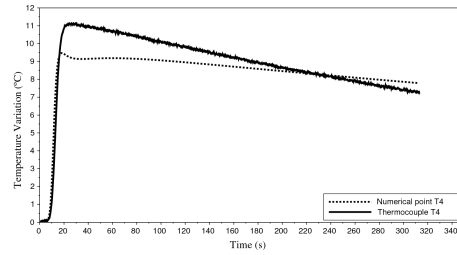
(b) T2



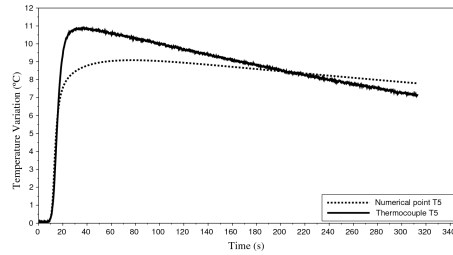
(c) T3



(d) T4



(e) T5



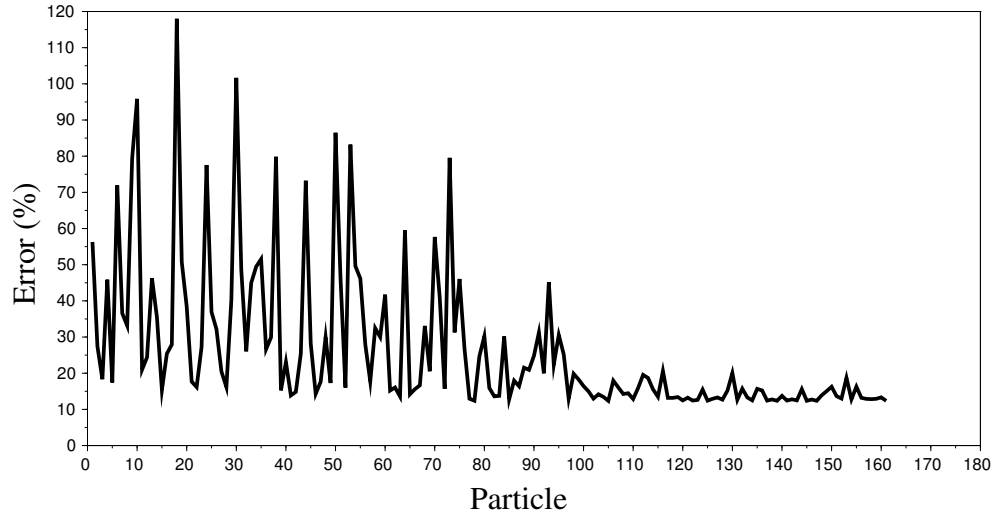
Source: Author's production, 2017

5.3 Linear Distribution

In the optimization process, the error between numerical and experimental temperatures is used to identify the coefficients. However, due to the PSO characteristics, the error isn't improved linearly. This variation can be seen in the Figure 25. The results convergence can be observed looking for a decrease of the peaks. The process was ended by the criterion of the minimum objective value change at the 161st particle. The procedure error found was $err_{proc} = 12.35 \%$.

In this distribution, a heat flux distribution with an uniform part and a linear part was considered, as represented in the Figure 15. In this distribution, the model coefficients of Q_{wp} are a and Q_{max} , and they are determined trough the inverse approach that was presented in the section 3.3. The best results found are $Q_{max} = 585524.1 \text{ W/m}^2$ and $a = 0.00289 \text{ m}$. After the heat flux identification, the average error between measured and

Figure 25 – Error variation along the optimization process



Source: Author's production, 2017

numerical temperatures was calculated. It was used the same equation that calculate the procedure error (Equation 3.1), but it was used more points as described in section 3.4. The average error is $err_{av} = 8.58 \%$.

The Figure 26 compares the workpiece temperature variation obtained for numerical simulation with experimental results. In the numerical curves, it can be observed that after 140 s the temperature tends to the same value in all curves, $\Delta T = 8.4 K$, while at the same instant in the experimentally measured there is a bigger difference.

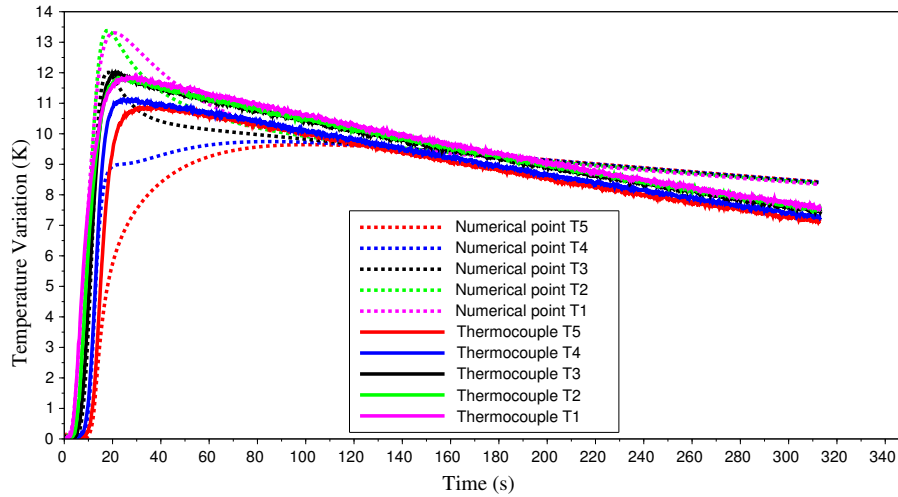
The error is different for each thermocouple analyzed, these results are presented in the Table 8. The smallest error is found in the input point T1 and the highest error is in the point T5, this information shows the better accuracy at the temperature estimation of the initial points.

Table 8 – Average error at each temperature using linear distribution

Temperature	T1	T2	T3	T4	T5
Average error (%)	5.87	6.29	7.25	9.55	13.95

Source: Author's production, 2017

Figure 26 – Numerical and experimental temperature in all thermocouples using linear distribution

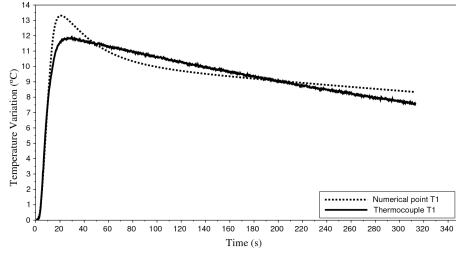


Source: Author's production, 2017

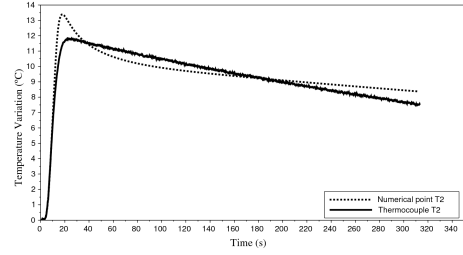
Looking to each temperature separately, (Figure 27) it can be seen some differences between the temperatures behavior. The numerical temperature in T1, T2, and T3 have a similar behavior to the experimental. In T4 and T5, the maximum temperature variations of the experimental results aren't reached by the numerical solution and the temperature decay is different. The highest error in the inferior thermocouples (T4 and T5) are associated with the heat loss by conduction to the machining fixing. This heat loss is inconsiderate in the FEM.

Figure 27 – Experimental and numerical temperatures using the linear distribution

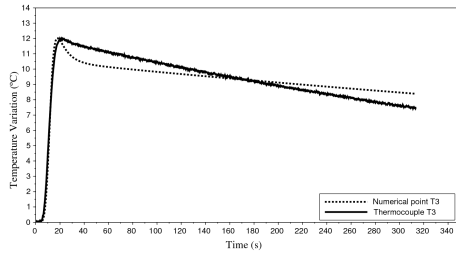
(a) T1



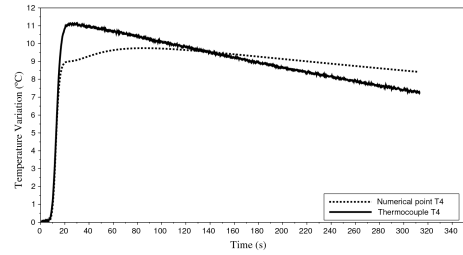
(b) T2



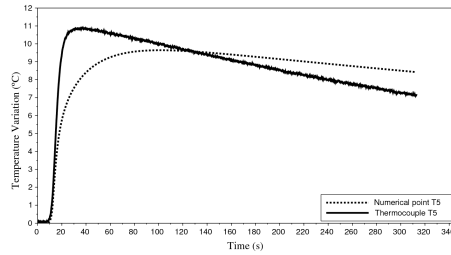
(c) T3



(d) T4



(e) T5



Source: Author's production, 2017

5.4 Polynomial Distribution

In this distribution, the heat flux Q_{wp} is defined by Equation 4.28 with 7 coefficients, c_0 , c_{11} , c_{12} , c_{21} , c_{22} , c_{31} , c_{32} . The value of the coefficient c_0 defines the initially uniform distributed Q_{wp} . All the coefficients were solved using the inverse procedure that was previously presented. The results are presented in the Table 9.

Table 9 – Polynomial Coefficients

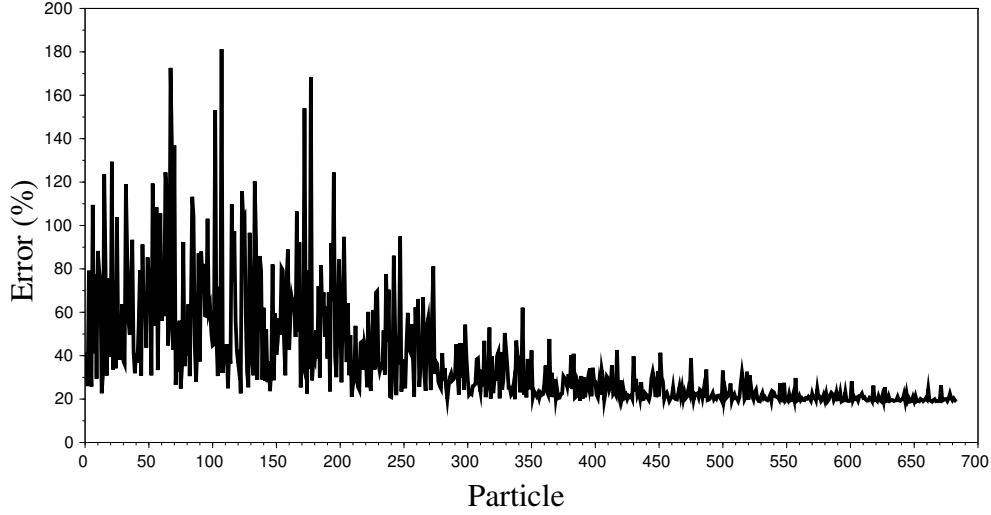
Coefficient	c_0	c_{11}	c_{12}	c_{21}	c_{22}	c_{31}	c_{32}
Result (kW/m)	100	302.28	-8.99	77.62	-10.0	78.77	4.06

Source: Author's production, 2017

The Equations 3.1 and 3.2 were used as error function, the inverse procedure found a value of $err_{proc} = 18.79\%$. The error convergence along the simulation process is

presented in the Figure 28. The coefficient values were found through the inverse approach that stopped by the criterion of the minimum objective value change.

Figure 28 – Error variation along the optimization process



Source: Author's production, 2017

The value of the control point Q_1 is the peak and increases steadily as the drill penetrates in the workpiece. The control points Q_2 also have a similar behavior, but the point Q_3 is different. The third control point is located at the point $y_3 = 30 \text{ mm}$ and it is activated at the step 120, $t = 7.44 \text{ s}$. The value of Q_3 decreases in time. These points were interpolated to find the heat flux distribution.

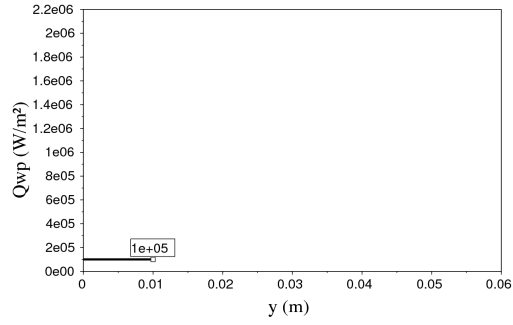
The Figure 29 shows the heat flux applied to the workpiece surface at different steps. In this graph, the reference $y = 0$ is the top surface of the workpiece and y is the hole in that step. The maximum value is in the tip of the drill whose position varies at each step because it is simulating the drilling.

Figure 30 shows the calculated and measured temperature variation to the five thermocouples using the polynomial distribution. This distribution also presented good results, the error is different to each curve but follows a difference tendency then that was found in the linear distribution. The numerical solution stabilizes at the temperature variation $\Delta T = 8.3 \text{ }^\circ\text{C}$.

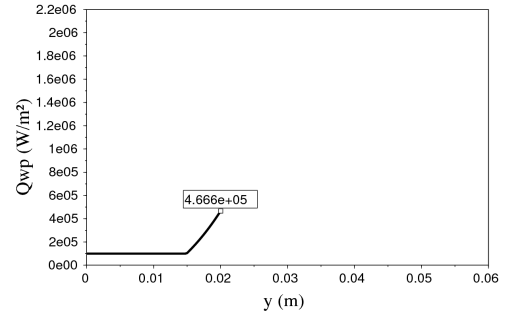
The average error is different at each temperature. In the Table 10 are presented the calculated errors between the numerical and experimental curves in the five thermocouples. The curve with the best result is T2 that presented $err = 7.57 \%$ and the worst result is T1 with an error $err = 10.73 \%$. It was different to what was found in the linear distribution. This difference to the linear distribution happens because the heat input in the beginning

Figure 29 – Heat flux in the polynomial distribution

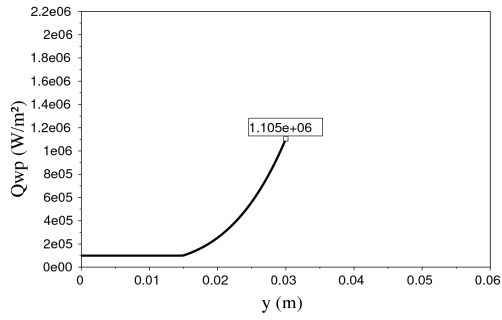
(a) 2.48 s



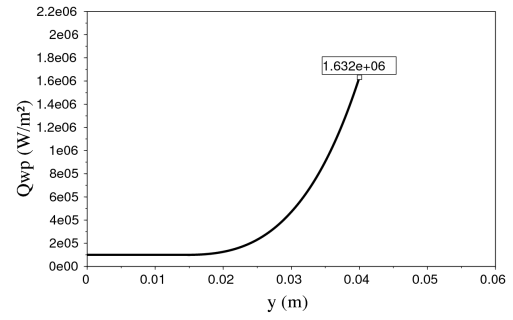
(b) 4.96 s



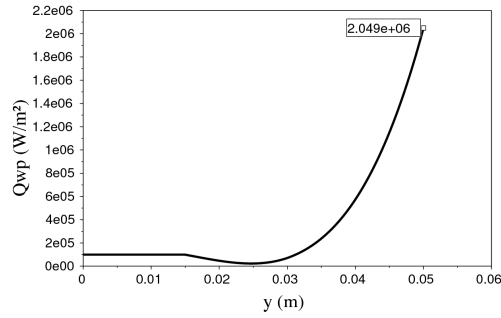
(c) 7.44 s



(d) 9.92 s



(e) 12.4 s



Source: Author's production, 2017

of the distribution isn't high enough to properly describe the real heat flux. The average error in this distribution is $err_{av} = 8.76 \%$.

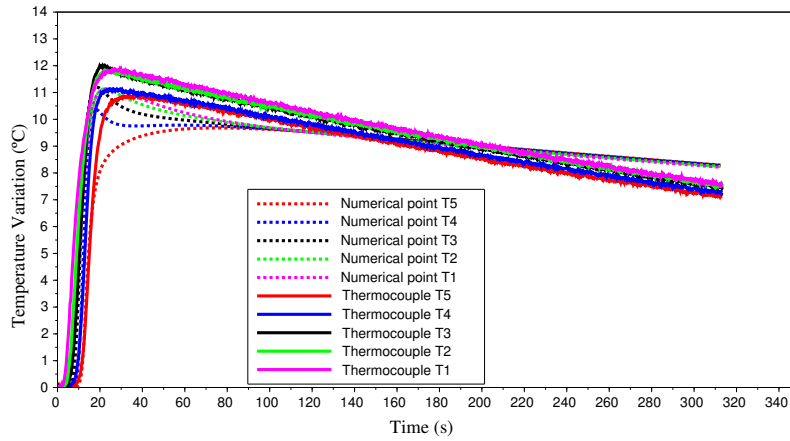
Table 10 – Average error at each temperature using polynomial distribution

Temperature	T1	T2	T3	T4	T5
Average error (%)	10.46	7.57	8.34	8.23	9.21

Source: Author's production, 2017

In the Figure 31, the simulated and measured temperature variation to each

Figure 30 – Numerical and experimental temperature in all thermocouples using polynomial distribution

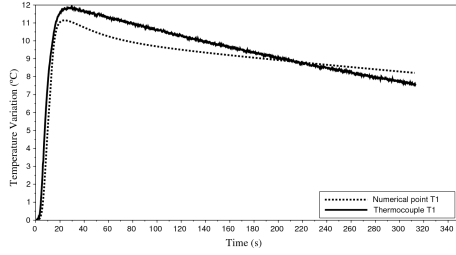


Source: Author's production, 2017

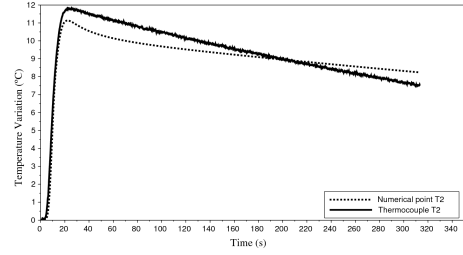
thermocouple are presented separately. Like in the concentrated distribution, in any of the simulated results the temperature variation reaches the maximum experimental value. However, the behavior of the temperatures in four of the thermocouples (T1, T2, T3, and T4) is similar to the experimental. As in the other distributions, the numerical result of T5 diverges from the experimental.

Figure 31 – Experimental and numerical temperatures using the polynomial distribution

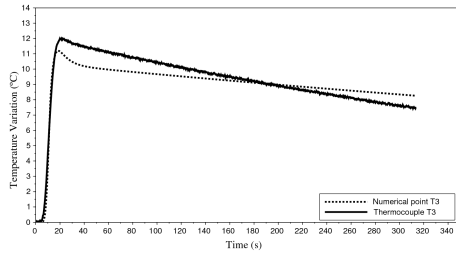
(a) T1



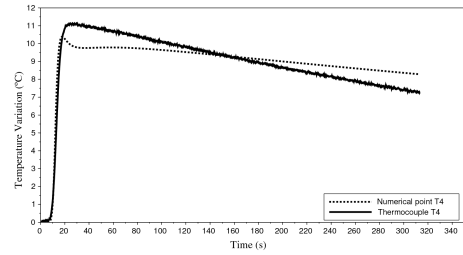
(b) T2



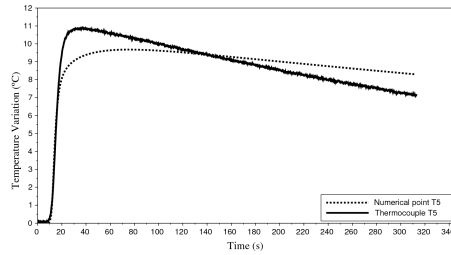
(c) T3



(d) T4



(e) T5



Source: Author's production, 2017

5.5 Hybrid Distribution

This distribution is a combination of two heat fluxes. In total, eight coefficients are used to define the heat flux to workpiece. The seven coefficients that were used at the polynomial distribution are combined with an additional coefficient, Q_0 . The additional coefficient defines a concentrated heat flux at the beginning of distribution.

The inverse procedure of heat flux identification was used to discover the value of all coefficients. At the end of the simulation, an error was determined using the error equation, $err_{proc} = 8.29 \%$, when the process was ended the following coefficient's values were found.

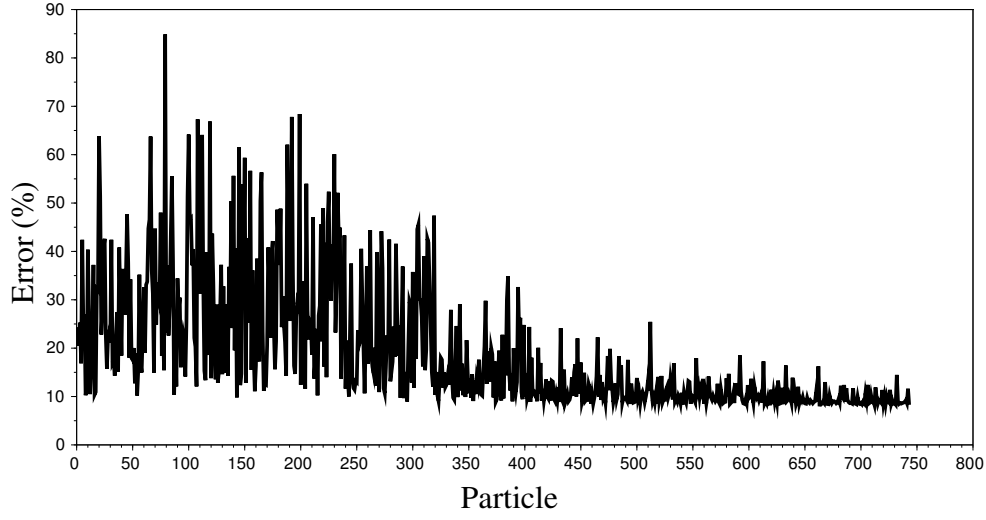
The inverse procedure found that error in the 743rd particle. The error of the particles' result was plotted in the Figure 32 and the peaks show the procedure's convergence. The stop criterion was the minimum variation of the objective function's value.

Table 11 – Hybrid coefficients

Coefficient	Q_0/m	c_0	c_{11}	c_{12}	c_{21}	c_{22}	c_{31}	c_{32}
Result (kW/m)	2616.88	97.40	50.00	6.76	27.27	-7.92×10^{-2}	49.37	-9.93

Source: Author's production, 2017

Figure 32 – Error variation along the optimization process



Source: Author's production, 2017

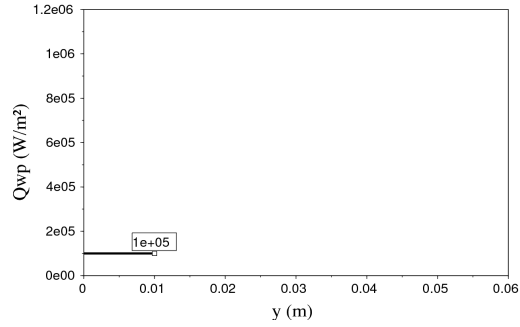
The portion of the heat flux that is controlled by the polynomial coefficients was interpolated and plotted in five different step times. The control point Q_1 is the peak and all the control points have your value increased with the time. The heat flux stages can be seen in the Figure 33, where $y = 0$ is the top surface of the workpiece. Due to the flux applied by the coefficient Q_0 , the flux defined by the polynomial coefficients is lower than in the approach that uses only the polynomial distribution.

The temperature calculated all thermocouples using the hybrid heat flux was plotted together with the experimental results. These temperature curves can be seen in the Figure 34. The average error of the simulation is $err_{av} = 7.34 \%$. The simulated temperatures stabilize at the variation $\Delta T = 8.3 K$ at 320 s and like in the other simulations the curves have different errors.

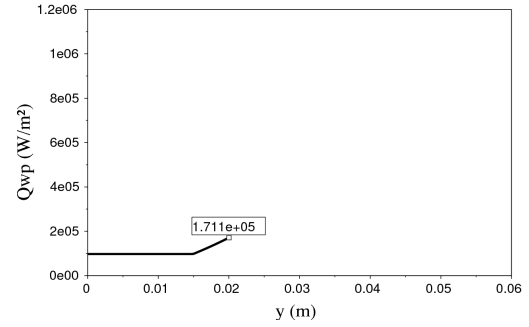
The average error was calculated using the Equations 3.1 and 3.2. The Table 12 shows the results to the distribution. The best result is in thermocouple T2, $err = 5.79 \%$, the result of thermocouple T1 is close to this and only T5 has an error above than 10 %. The error increases according to the depth at which the thermocouple is located.

Figure 33 – Polynomial fraction of heat flux in the hybrid distribution

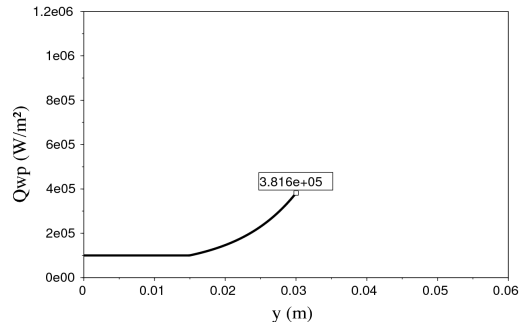
(a) 2.48 s



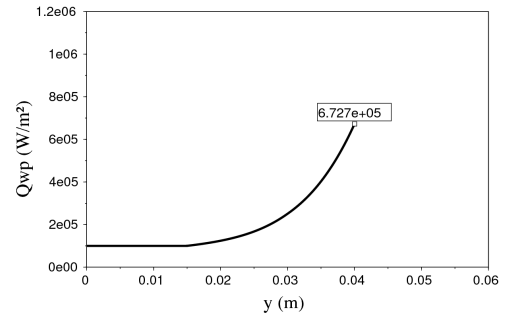
(b) 4.96 s



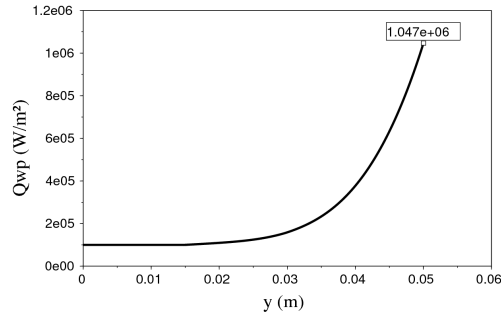
(c) 7.44 s



(d) 9.92 s



(e) 12.4 s



Source: Author's production, 2017

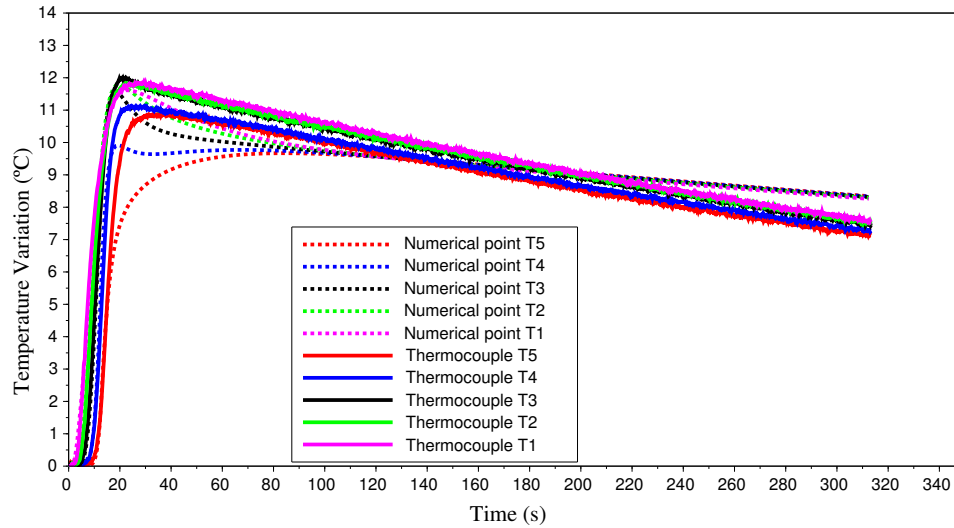
Table 12 – Average error at each temperature using hybrid distribution

Temperature	T1	T2	T3	T4	T5
Average error (%)	5.93	5.79	6.78	8.08	10.11

Source: Author's production, 2017

In the Figure 35, the simulated and measured temperature variation to each thermocouple is presented separately. In three thermocouples, (T1,T2, and T3) the maximum temperature variations calculated reach the measured temperature. In these

Figure 34 – Numerical and experimental temperature in all input points using hybrid distribution

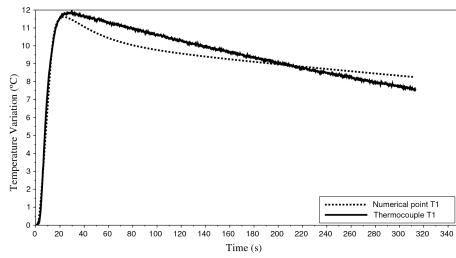


Source: Author's production, 2017

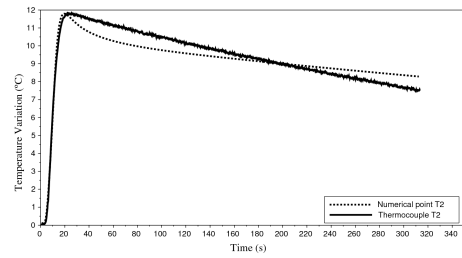
temperatures, the behavior is similar in numerical and experimental results. The behavior is also similar in T4. As in the other distributions, the numerical result of T5 diverges from the experimental.

Figure 35 – Experimental and numerical temperatures using the polynomial distribution

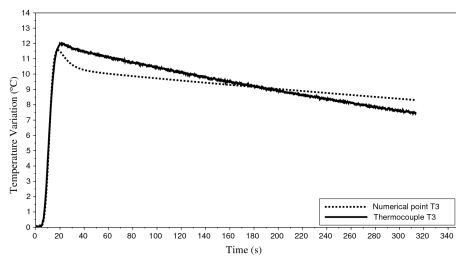
(a) T1



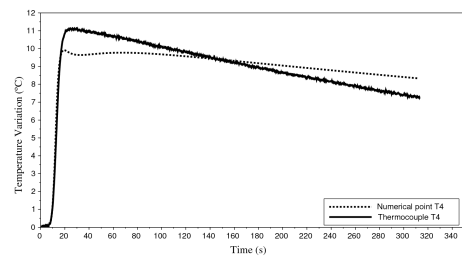
(b) T2



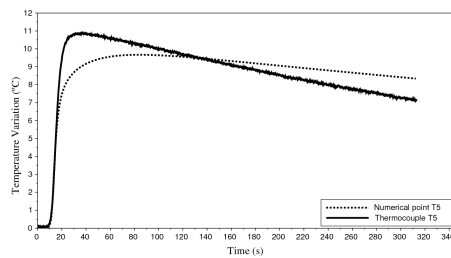
(c) T3



(d) T4



(e) T5



Source: Author's production, 2017

5.6 Comparison between the distributions

The first comparison between the results for each heat distribution, it is the difference in the average error, which can be seen at the Table 13. The hybrid distribution presented the best overall result among all proposed distributions. The three distributions that consider the heat transfer along the wall presented a better result than the concentrated heat flux.

Table 13 – Average error to each heat flux distributions

Distribution	Concentrated	Linear	Polynomial	Hybrid
Average error (%)	13.95	8.58	8.76	7.34

Source: Author's production, 2017

Using the experimentally measured torque, it is possible to calculate the total

heat generated in the machining process. This was already calculated in the section 5.2, $Q_{total} = 111147 \text{ J}$. In the FEM, the heat loss happens only through natural convection. If the convection is disregarded, all the applied heat remains in the workpiece. The workpiece tends to thermal equilibrium, when the workpiece reaches the thermal equilibrium it is possible to calculate the heat transferred to the workpiece using the Equation 5.1.

$$Q_{wp} = mc_p \Delta T \quad (5.1)$$

where $m = 0.656 \text{ kg}$ is the workpiece mass, $c_p = 490 \text{ KJ/KgK}$ is the specific heat and ΔT is the temperature variation .

Analyzing the distributions used in this research the heat transferred to the workpiece is around 30 % as shown in the Table 14. This result proves that the magnitude of the heat fluxes that were determined through the inverse procedure are according to the literature.

Table 14 – Heat flux transferred to workpiece

Distribution	Heat transferred to workpiece (J)	Percentage of the heat generated (%)
Concentrated	3352.8	30
Linear	3375	30.2
Polynomial	3311	29.6
Hybrid	3324	29.7

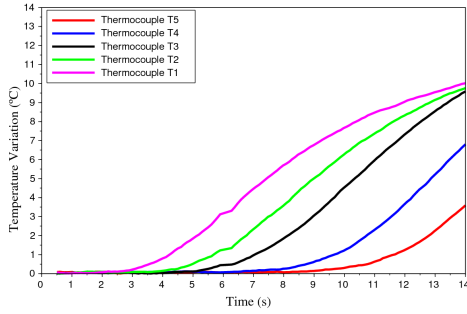
Source: Author's production, 2017

The initial temperature variation has some differences between experimental and numerical results. The Figure 36 shows the firsts 14 s of each result. Differently from the experimental result, the numerical temperature variations in T2 and T3 surpass the value of T1. This happens more sharply when the polynomial distribution is used. This difference in the behavior of the curves is due to the fact that in the numerical model the hole is considered as preexisting. Then a portion of the heat that should be conducted to the material not yet removed, it is transferred to the region of the thermocouples causing a higher temperature rise.

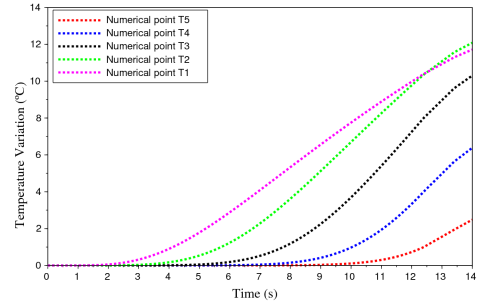
The differences in the distributions can be seen in the Figure 37. The figure shows the workpiece temperature for each distribution. The way that the heat disperses through the workpiece differs according to the distribution used. The highest temperatures are found in the polynomial distribution. However, due to the distribution of the heat flux, between the bottom of the workpiece, where the temperature peak is, and the top of the workpiece, there is a region with low temperature.

Figure 36 – Initial temperature variation in each distribution

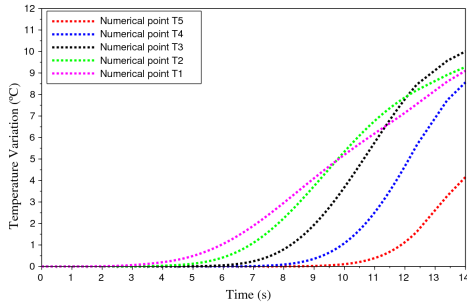
(a) Experimental



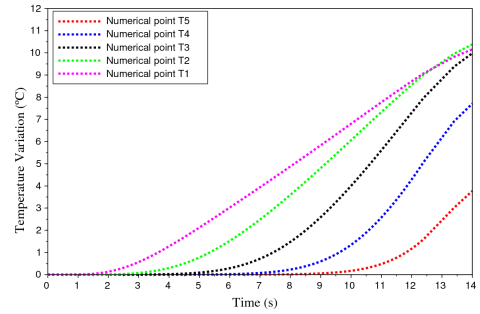
(b) Linear



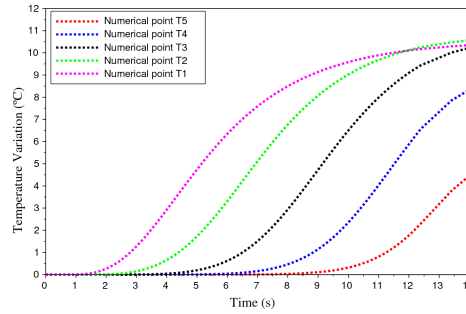
(c) Polynomial



(d) Hybrid



(e) Concentrated



Source: Author's production, 2017

The temperature distribution for the hybrid flux is the most uniform. While in linear distribution the temperature ends up having a parabola distribution with the temperature change wave spreading faster in the central region in the hybrid heat flux this change further follows the movement of the tool in the process with the temperature wave reaching the outer face first in the upper part.

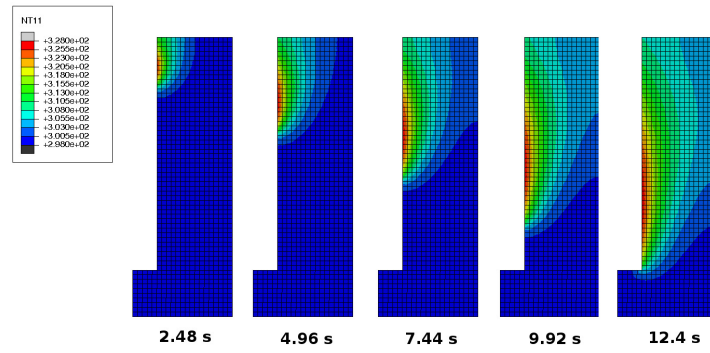
The lowest temperatures occur in the concentrated flow, comparing its results with the result of the distributions that consider the heat flux along the machined surface, one can perceive the influence that this consideration generates on the temperature distribution.

From this information, it is possible to perceive the influence of the distribution of the heat flow. Although all flows transfer almost the same amount of heat to the part, there are significant differences due to the distribution. In the concentrated flow, one notices how the temperature start is very anticipated. At the same time, in the curves of the linear distribution, we notice a delay that is due to the lack of a peak of heat flow at the beginning of the distribution. The linear and hybrid distributions show a good accuracy in the rise of the temperature curves with their results being very close to the experimental result.

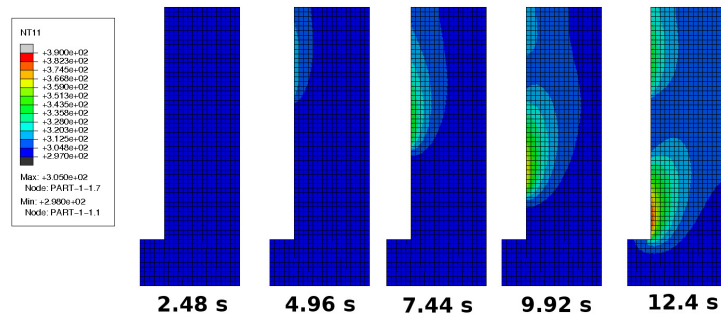
A comparison between the distributions is done analyzing the results for thermocouples T1, T3, and T5. These temperatures were chosen due to the thermocouples' location.

Figure 37 – Workpiece temperature distribution to different heat flux distributions

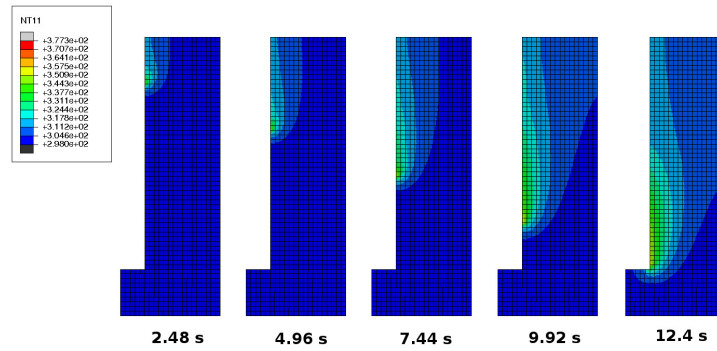
(a) Linear



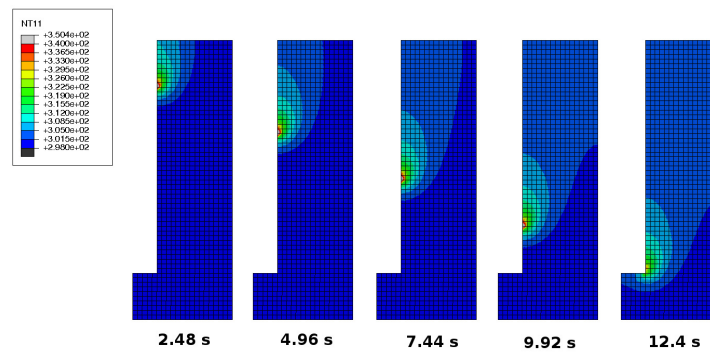
(b) Polynomial



(c) Hybrid



(d) Concentrated

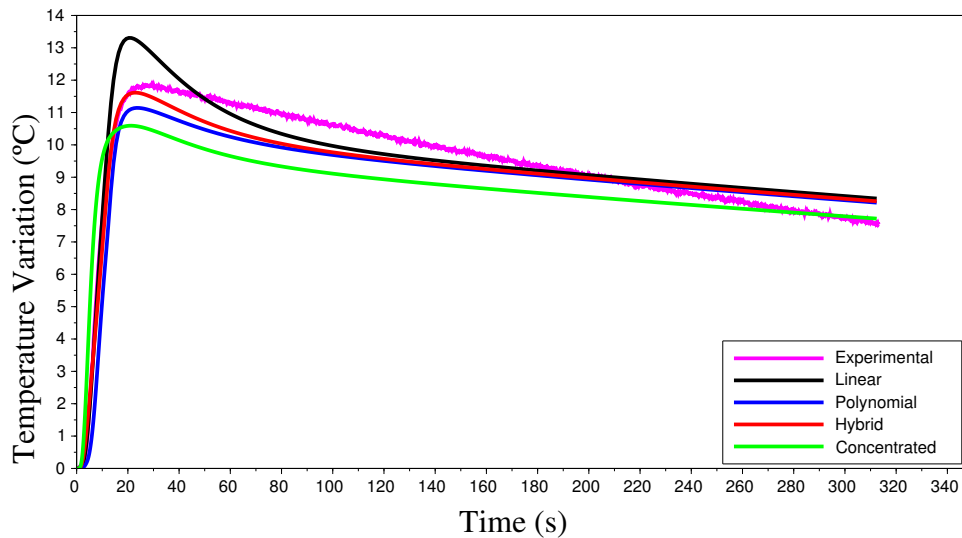


Source: Author's production, 2017

5.6.1 Thermocouple T1

Analysing all the results at the thermocouple T1, which are presented in Figure 38, it is possible to observe some differences. The curve of the linear distribution has a maximum value that is higher than in others distributions. The temperatures for hybrid and polynomial distributions have behaviors that are closer to experimental than others distributions. The difference is also evidenced when we analyze the average error of the thermocouple T1 for each heat distribution (Table 15). The linear and hybrid heat fluxes have errors that are almost half the error found for the concentrated and polynomial distributions.

Figure 38 – Experimental and numerical temperatures in T1



Source: Author's production, 2017

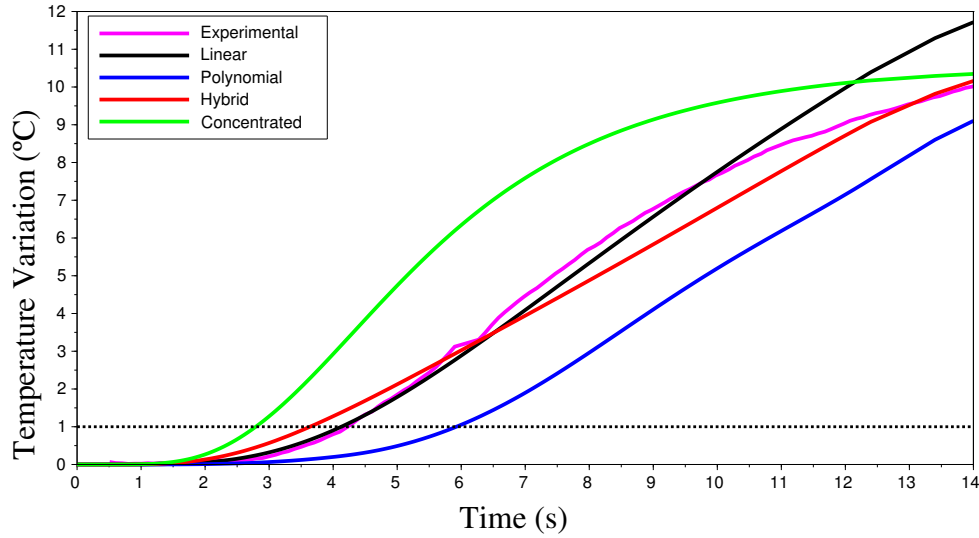
Table 15 – Average error in T1 to each heat flux distributions

Distribution	Concentrated	Linear	Polynomial	Hybrid
Average error (%)	10.24	5.87	10.45	5.93

Source: Author's production, 2017

In the Figure 39, it can be observed that the initial behavior of the linear and hybrid fluxes are closer to the experimental results than other two approaches. The polynomial presents the greatest delay due to the low value at the beginning of the flux. While the result for the concentrated heat suffers from a faster temperature variation. The reaction times to each distribution are presented in the Table 16. This reaction time is affected by the magnitude of the heat flux in the region near drill tip. The concentrated has the lowest value because all the heat flux is concentrated in a small region near the drill tip.

Figure 39 – Experimental and numerical temperatures in T1



Source: Author's production, 2017

Table 16 – Reaction times for temperatures in T1

Distribution	Experimental	Linear	Polynomial	Hybrid	Concentrated
Reaction time (s)	4.2	4.1	5.9	3.7	2.8

Source: Author's production, 2017

Another characteristic that was compared, it is the maximum temperature variation in T1. In the Table 17, it can be seen this value and the instant time, that is the time when the temperature variation reaches his maximum. The maximum temperature in hybrid approach has the closest result to the experimental and it presented the same instant time of experimental results.

Table 17 – Maximum temperature variations in T1

	Experimental	Linear	Polynomial	Hybrid	Concentrated
Maximum temperature variation (°C)	11.9	13.3	11.1	11.6	10.6
Instant time (s)	22.4	20.4	21.4	22.4	21.4

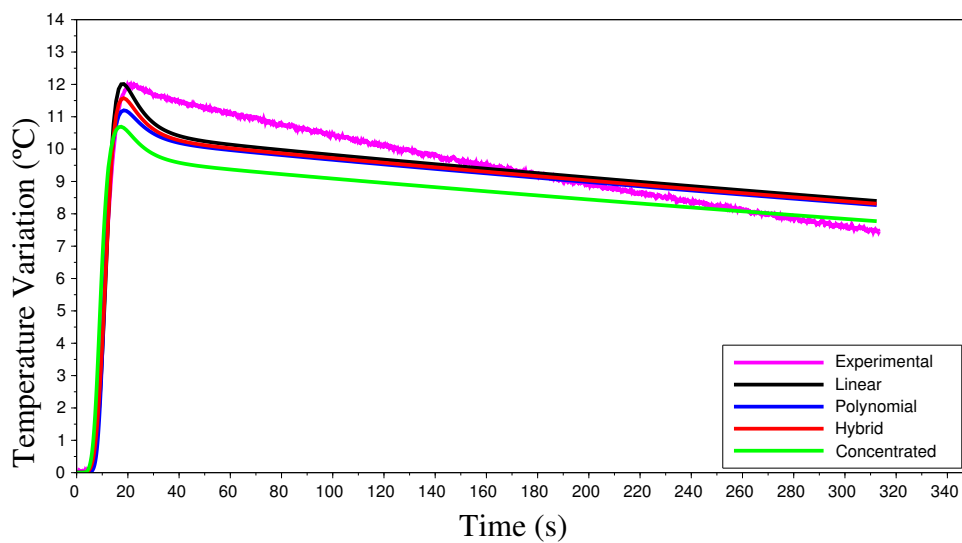
Source: Author's production, 2017

5.6.2 Thermocouple T3

Looking at the temperature variations in T3 that are presented in the Figure 40, it can be observed similar results to linear, polynomial and concentrated distributions. The

concentrated approach presented temperatures that are lower than in the other approaches. The average error, which is presented in Table 18, shows that hybrid distribution also has the best result in this thermocouple. However, it was only in the concentrated distribution that the error was higher than 10 %, the linear an polynomial have errors that are close to the hybrid result.

Figure 40 – Experimental and numerical temperatures in T3



Source: Author's production, 2017

Table 18 – Average error in T3 to each heat flux distribution

Distribution	Concentrated	Linear	Polynomial	Hybrid
Average error (%)	11.80	7.25	8.34	6.78

Source: Author's production, 2017

The beginning of the temperature variation measured in thermocouple T3 and the simulated results follows the same trend that was observed in T1. The Figure 41 shows these results. The reaction times can be seen at Table 19. They follow the same order that in T1, when organized from the smallest to the longest: concentrated, hybrid, linear and polynomial.

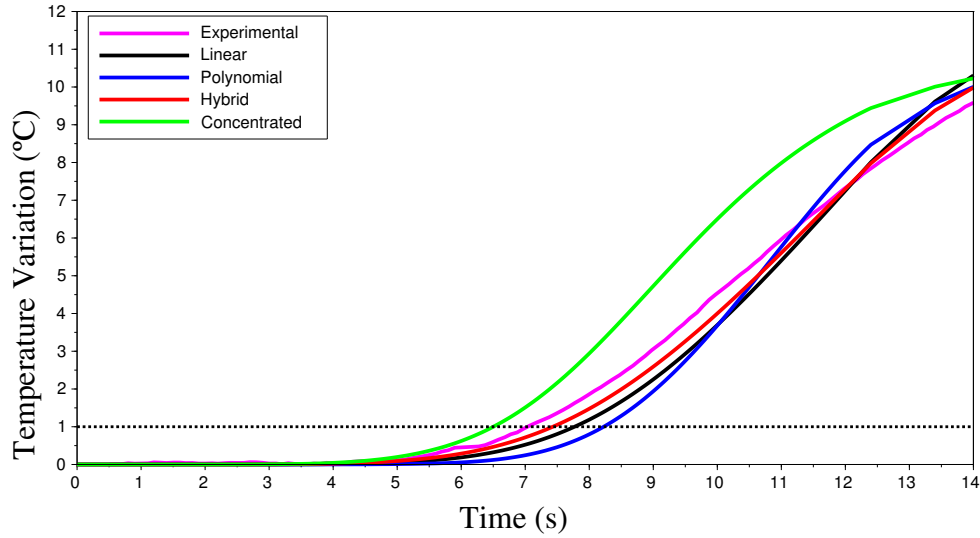
Table 19 – Reaction times for temperatures in T3

Distribution	Experimental	Lienar	Polynomial	Hybrid	Concentrated
Reaction time (s)	7.0	7.8	8.2	7.4	6.5

Source: Author's production, 2017

The maximum temperature variation in T3 can be seen at the Table 20. The experimental and numerical results are similar in this case. The concentrated distribution

Figure 41 – Experimental and numerical temperatures in T3



Source: Author's production, 2017

has the highest difference, but the other distributions have results closer to the experimental. The linear reaches the same maximum value to the temperature variation with a difference in the instant time. This instant time, 18.4 s, is the same to polynomial and hybrid. This shows that in the simulations the temperature variation is more pronounced than in the experimentally measured result because, despite the delay in the beginning of the variation, it reaches the maximum before.

Table 20 – Maximum temperature variations in T3

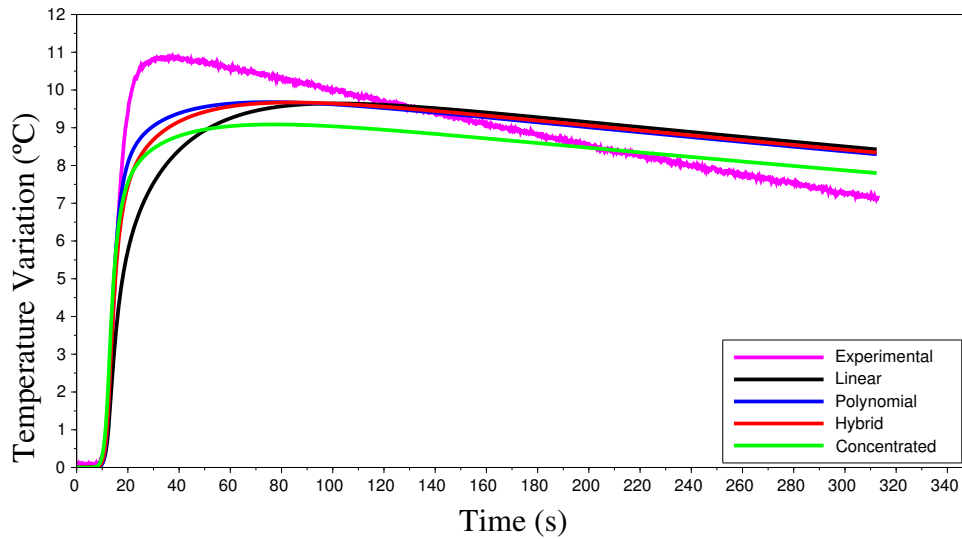
Distributions	Experimental	Linear	Polynomial	Hybrid	Concentrated
Maximum temperature variation (°C)	12.0	12.0	11.2	11.6	10.7
Instant time (s)	20.4	18.4	18.4	18.4	17.4

Source: Author's production, 2017

5.6.3 Thermocouple T5

At the Figure 42 can be seen the measured and simulated temperature variations in T5. The thermocouple T5 presents the worst error in comparison with the others thermocouples. The exception is the polynomial distribution, in which T5 is the thermocouple with the lowest error. The average error in T5 to each distribution can be seen at the Table 21.

Figure 42 – Experimental and numerical temperatures in T5



Source: Author's production, 2017

Table 21 – Average error in T5 to each heat flux distribution

Distribution	Concentrated	Linear	Polynomial	Hybrid
Average error (%)	18.45	13.95	9.21	10.11

Source: Author's production, 2017

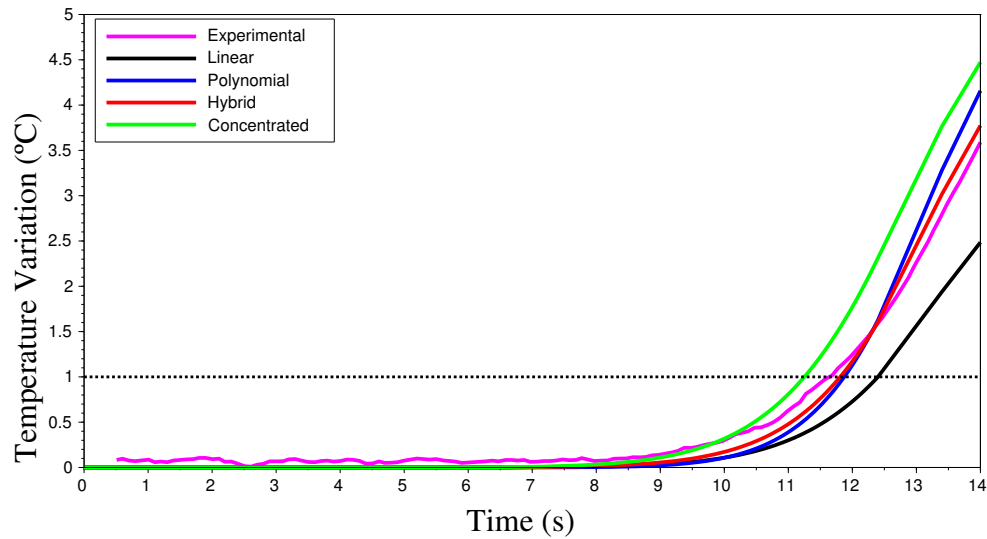
The Figure 43 shows the initial temperature variation in T5. It presents a difference in relation to T1 and T3. The polynomial distribution result is closer to the experimental than was observed in the other thermocouples. For the other distributions, the results follow the same trend. The values of the experimental reaction time and of each distribution can be seen in the Table 22.

Table 22 – Reaction times for temperatures in T5

Distribution	Experimental	Lienar	Polynomial	Hybrid	Concentrated
Reaction time (s)	11.6	12.3	11.9	11.8	11.3

Source: Author's production, 2017

Figure 43 – Experimental and numerical temperatures in T5



Source: Author's production, 2017

In the maximum temperature variation, there is a difference higher than in other thermocouples. As can be seen in the Table 23, all the numerical results are close to each other, but it has more than 1-degree difference for the experimental. In addition, the instant where the simulation reaches the maximum temperature variation occurs around 30 s after the maximum experimental value. These results demonstrate the difficulty in all numerical models of representing the temperature at the bottom of the workpiece.

Table 23 – Maximum temperature variations in T5

Distributions	Experimental	Linear	Polynomial	Hybrid	Concentrated
Maximum temperature variation (°C)	10.9	9.6	9.7	9.6	9.7
Instant time (s)	34.4	80.4	62.4	60.4	69.4

Source: Author's production, 2017

6 Conclusions

During the machining process, there is heat generation at the tool tip due to the plastic deformation of the material. The heat is also generated due to the friction between the chip, the tool and the workpiece. This heat propagates to chip, tool, and workpiece causing thermal deformations, which is a source that generates errors in the process. In dry machining due to the lack of cutting fluid, this condition becomes critical. In the drilling process, the thermal problem becomes critical because the drill bit is enclosed in the hole. This complicates the dissipation of the generated heat. The identification of the heat flux flowing to the workpiece allows the calculation of the workpiece temperature distribution.

There are several approaches in the literature to calculate heat flux and temperature in the drilling, among them the FEM. Within this method, there are different approaches for the heat flux distribution. As discussed in Chen et al. (2017) four different strategies to thermal load can be used: advection model, surface heat model, heat carrier model and ring heat model.

The models that use element deletion in spite of presenting good results have a very high computational cost. This may do the use of this approach unfeasible in some cases. In the case of models that use a preexisting hole, the heat distribution is usually considered constant. Flux variations are usually not considered and there is no consideration of heat flux along the hole wall. Tai et al. (2012) considered the distribution of the heat flux along the wall and the variation of the flow over time. However, the author used the element deletion and still identified the total flux in two separate procedures. This turns the overall procedure very costly.

In this work, the methodology adopted considered a model with a preexisting hole but also considered a variation in the heat flux over time. Using the experimentally measured workpiece temperature, combining with the finite element model, the heat flux flowing to the workpiece was identified. Using the PSO in the inverse procedure, the error between the experimental and numerical values was minimized for three different heat flux distributions. A fourth distribution, that treats the flux as concentrated in a small area, was calculated analytically and used for comparison purposes with the proposed models.

To obtain the required experimental data, a cylindrical workpiece was drilled using the dry drilling process. The temperature was recorded using thermocouples coupled to the workpiece surface. This workpiece was modeled ABAQUS and the different heat flux distributions were applied.

The results obtained for the three distributions, identified in the inverse procedure, were satisfactory. The results are specially goods onsidering the simplifications of the

numerical model and the experimental measurement. All distributions presented a mean square error less than 9 %. The distribution that presented the best result was the hybrid , $err_{av} = 7.34$ %.

The curve fitting for T5 had the biggest errors overall. Even in the polynomial distribution that presented the best result for this curve, the error was close to 10 %. In contrast, it is in the polynomial distribution that the worst result for T1 ($err_{av} = 10.11$ %) was found. While in the linear and hybrid distributions the errors were respectively 5.87 % and 5.93 % .

The linear and hybrid distributions were those that were closer to experimental at the beginning of the temperature variations. The concentrated heat flux is the one that had the most advanced heating, while in the polynomial distribution the heating presented a delay. This showed that the beginning of the temperature variatio is mainly influenced by the value of the heat flux in the drill tip. In the concentrated flu, the heat in the drill tip is the greater of all distributions and in the polynomial is the smaller value. They had respectively the smallest and the biggest reactions times.

The amount of heat that was transferred to the workpiece was in agreement with the values found in the literature. In the three distributions, the value was around 30 % which is in agreement with the literature that places the amount of heat transferred to the workpiece between 10 and 35 % for dry drilling (FLEISCHER et al., 2007).

At the end of the analyzes, it can be concluded that the hybrid distribution was the one with the best results. Besides the smaller average error, the behavior of the curves, especially in the initial temperature variation, was very close to the experimental. Segurajauregui and Arrazola (2015) despite presenting a minor error, 3.65% used the advection model which is more complex and also analyzed a shorter time without evaluating the cooling phase. As seen in the results, there is an increase in the error in the end of simulation due to the experimental limitation.

Finally, it can be concluded that the proposed approach is able to satisfactorily identify the heat flux flowing to the workpiece during dry drilling, without the need for large computational costs or complex experimental tests.

6.1 Suggestions for Future Works

Some suggestions for future works which can help in the improvement of the dry machining process.

The experimental setup presented some limitations and contributed to the errors of the analysis. A good isolation between workpiece and machine fixture would ally the finite element model represent with more accuracy the system behavior.

The use of the methodology applied in this work to be able to calculate the temperature of the workpiece in wet and mql drilling would provide important data to compare the effects of the application of cutting fluid.

Using the inverse procedure of this work for drilling with other machining parameters would help to develop the method and discover possible limitations of its application. A similar approach could also be used for other machining processes such as turning.

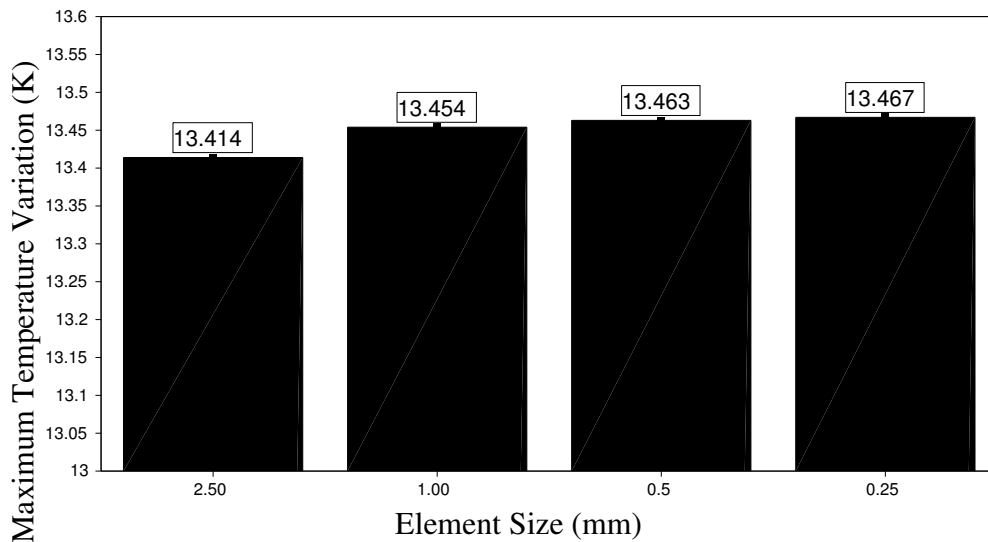
There is also the possibility of studying the efficiency of this model in the case of workpieces that are submitted to several sequential holes, analyzing what considerations would be necessary to fit the model.

A Mesh refinement

The influence of the finite element parameters as element size and time integration were analysed before the iterative analysis to identify the heat flux. The mesh refinement was done with a heat source defined by an uniform part and a linear part. The element sizes used in the simulations were $E_1 = 2.5 \text{ mm}$, $E_2 = 1 \text{ mm}$, $E_3 = 0.5 \text{ mm}$ and $E_4 = 0.25 \text{ mm}$.

This sizes were chosen because the temp points analysed can be the same in the experimental tests. In these analysis were used the time steps $\Delta_{t,d} = 0.1 \text{ s}$ and $\Delta_{t,c} = 2.0 \text{ s}$. As can be seen in the figure 44, the element size has a small influence in the maximum temperature, the maximum temperature variation has a difference smaller than 1 %. It was chosen the element size $S_2 = 1 \text{ mm}$ because this size generates a mesh with little distortion and the time simulation isn't so high.

Figure 44 – Influence of element size in the maximum temperature variation simulated



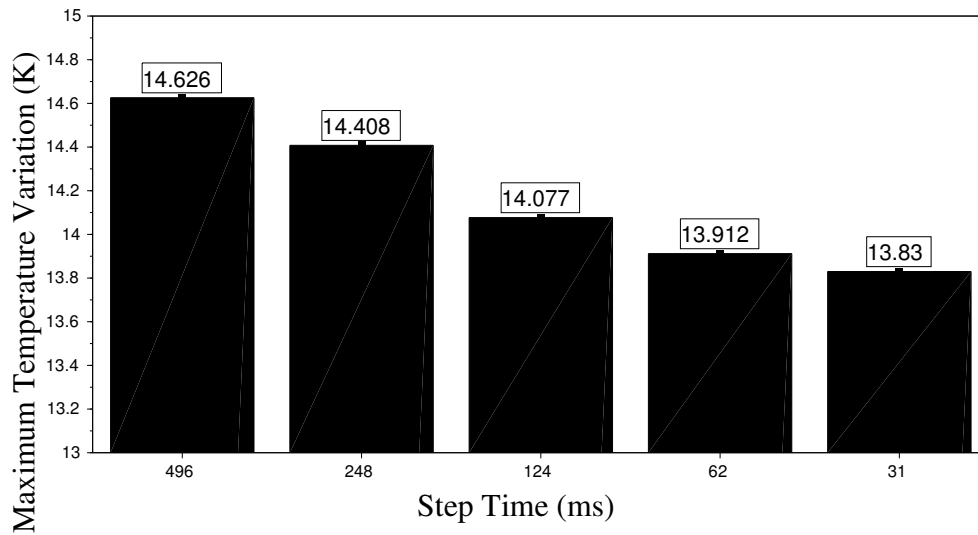
Source: Author's production, 2017

The step time influence was analysed separately in drilling and cooling phase. In drilling phase the time step was chosen based in the total drilling time, that is 12,4 s. The first step time used was the time required for the tool to drill 2 mm. This step time is $\Delta_{t,d_1} = 496 \text{ ms}$, the other step times were defined as $\Delta_{t,d_1}/2$, $\Delta_{t,d_1}/4$, $\Delta_{t,d_1}/8$ and $\Delta_{t,d_1}/16$.

In these analyzes the other parameters were $S = 1 \text{ mm}$ and $\Delta_{t,c} = 2.0 \text{ s}$. In the time discretisation of the first step the maximum temperature variation decreases as step time

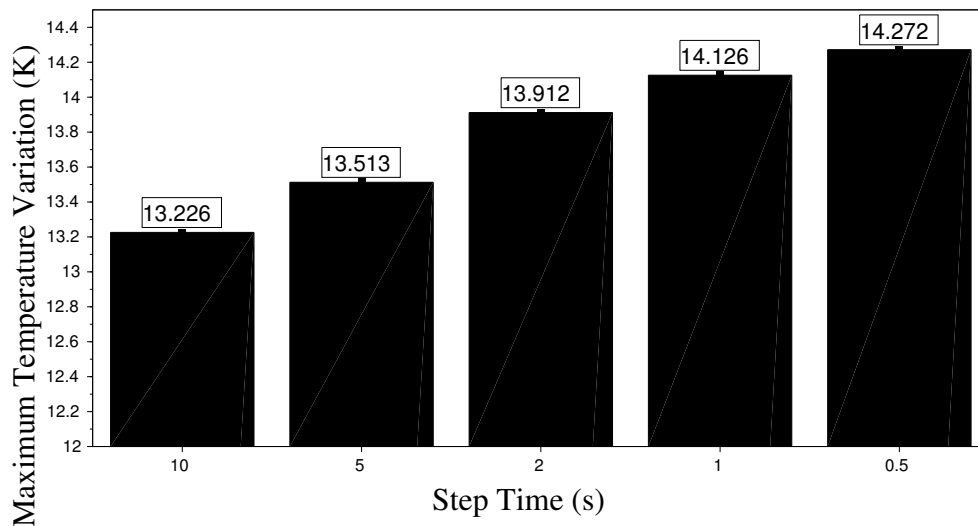
decreases as can be seen in figure 45. The defined step time was $\Delta_{t,d} = 62ms$, because reducing the time step to $\Delta_{t,d} = 31ms$ resulted in a relative decrease of less than 1 % and the processing time is the double.

Figure 45 – Influence of drilling step time in the maximum temperature variation simulated



Source: Author's production, 2017

Figure 46 – Influence of cooling step time in the maximum temperature variation simulated



Source: Author's production, 2017

In the cooling phase five different time steps were analysed as can be seen in figure 46. The shorter the time step the higher the temperature variation in the workpiece. The temperature increasement between the time steps $\Delta_{t,c} = 1.0s$ and $\Delta_{t,c} = 0.5s$ was only 1%,

but the computer time required was increased in almost 100 % because of this $\Delta_{t_c} = 1.0s$ was defined as an appropriated time step to this phase.

Bibliography

ABUKHSHIM, N.; MATIVENGA, P.; SHEIKH, M. Heat generation and temperature prediction in metal cutting: A review and implications for high speed machining. *International Journal of Machine Tools and Manufacture*, Elsevier, v. 46, n. 7, p. 782–800, 2006. Cited 2 times on pages 15 and 16.

AGAPIOU, J.; DEVRIES, M. On the determination of thermal phenomena during drilling—part i. analytical models of twist drill temperature distributions. *International Journal of Machine Tools and Manufacture*, Elsevier, v. 30, n. 2, p. 203–215, 1990. Cited on page 9.

AGAPIOU, J.; STEPHENSON, D. Analytical and experimental studies of drill temperatures. *TRANSACTIONS-AMERICAN SOCIETY OF MECHANICAL ENGINEERS JOURNAL OF ENGINEERING FOR INDUSTRY*, AMERICAN SOCIETY MECHANICAL ENGINEERS, v. 116, p. 54–54, 1994. Cited on page 10.

AURICH, J. C.; ZIMMERMANN, M.; SCHINDLER, S.; STEINMANN, P. Analysis of the machining accuracy when dry turning via experiments and finite element simulations. *Production Engineering*, Springer, v. 8, n. 1-2, p. 41–50, 2014. Cited on page 7.

BARADIE, M. E. Cutting fluids: Part ii. recycling and clean machining. *Journal of materials processing technology*, Elsevier, v. 56, n. 1-4, p. 798–806, 1996. Cited on page 1.

BATTAGLIA, J.; PUIGSEGUR, L.; CAHUC, O. Estimated temperature on a machined surface using an inverse approach. *Experimental heat transfer*, Taylor & Francis, v. 18, n. 1, p. 13–32, 2005. Cited on page 16.

BER, A.; GOLDBLATT, M. The influence of temperature gradient on cutting tool's life. *CIRP Annals-Manufacturing Technology*, Elsevier, v. 38, n. 1, p. 69–73, 1989. Cited on page 8.

BERGMAN, T. L.; INCROPERA, F. P. *Fundamentals of heat and mass transfer*. [S.l.]: John Wiley & Sons, 2011. Cited on page 21.

BIERMANN, D.; IOVKOV, I. Modeling and simulation of heat input in deep-hole drilling with twist drills and mql. *Procedia CIRP*, Elsevier, v. 8, p. 88–93, 2013. Cited on page 14.

BIERMANN, D.; IOVKOV, I.; BLUM, H.; RADEMACHER, A.; TAEBI, K.; SUTTMEIER, F.; KLEIN, N. Thermal aspects in deep hole drilling of aluminium cast alloy using twist drills and mql. *Procedia CIRP*, Elsevier, v. 3, p. 245–250, 2012. Cited on page 13.

BLANC, G.; RAYNAUD, M.; CHAU, T. H. A guide for the use of the function specification method for 2d inverse heat conduction problems. *Revue générale de thermique*, Elsevier, v. 37, n. 1, p. 17–30, 1998. Cited on page 16.

BONO, M.; NI, J. A model for predicting the heat flow into the workpiece in dry drilling. *Journal of Manufacturing Science and Engineering*, American Society of Mechanical Engineers, v. 124, n. 4, p. 773–777, 2002. Cited on page 12.

BONO, M.; NI, J. The location of the maximum temperature on the cutting edges of a drill. *International Journal of Machine Tools and Manufacture*, Elsevier, v. 46, n. 7, p. 901–907, 2006. Cited on page 11.

BOOTHROYD, G. Temperatures in orthogonal metal cutting. *Proceedings of the Institution of Mechanical Engineers*, SAGE Publications Sage UK: London, England, v. 177, n. 1, p. 789–810, 1963. Cited 2 times on pages 10 and 11.

CHEN, L.; TAI, B. L.; YANG, J. A.; SHIH, A. J. Experimental study and finite element modeling of workpiece temperature in finish cylinder boring. *Journal of Manufacturing Science and Engineering*, American Society of Mechanical Engineers, v. 139, n. 11, p. 111003, 2017. Cited 3 times on pages 12, 14, and 65.

CHEN, W.-C.; TSAO, C.-C.; LIANG, P.-W. Determination of temperature distributions on the rake face of cutting tools using a remote method. *International communications in heat and mass transfer*, Elsevier, v. 24, n. 2, p. 161–170, 1997. Cited on page 15.

CUI, M.; GAO, X.; ZHANG, J. A new approach for the estimation of temperature-dependent thermal properties by solving transient inverse heat conduction problems. *International Journal of Thermal Sciences*, Elsevier, v. 58, p. 113–119, 2012. Cited on page 16.

DAVIES, M.; UEDA, T.; M'SAOUBI, R.; MULLANY, B.; COOKE, A. On the measurement of temperature in material removal processes. *CIRP Annals-Manufacturing Technology*, Elsevier, v. 56, n. 2, p. 581–604, 2007. Cited on page 1.

DENG, S.; HWANG, Y. Applying neural networks to the solution of forward and inverse heat conduction problems. *International Journal of Heat and Mass Transfer*, Elsevier, v. 49, n. 25, p. 4732–4750, 2006. Cited on page 16.

DENKENA, B.; SCHMIDT, C.; KRÜGER, M. Experimental investigation and modeling of thermal and mechanical influences on shape deviations in machining structural parts. *International Journal of Machine Tools and Manufacture*, Elsevier, v. 50, n. 11, p. 1015–1021, 2010. Cited on page 8.

DOGU, Y.; ASLAN, E.; CAMUSCU, N. A numerical model to determine temperature distribution in orthogonal metal cutting. *Journal of Materials Processing Technology*, Elsevier, v. 171, n. 1, p. 1–9, 2006. Cited on page 10.

DORMER. *Dormer Catalogue*. [S.l.], 2015. Cited on page 22.

DUTT, R.; BREWER, R. On the theoretical determination of the temperature field in orthogonal machining. *International Journal of Production Research*, Taylor & Francis, v. 4, n. 2, p. 91–114, 1965. Cited on page 10.

FAVERJON, P.; RECH, J.; VALIORGUE, F.; ORSETTI, M. Optimization of a multi-drilling sequence with mql supply to minimize thermal distortion of aluminum parts. *Journal of Machine Engineering*, v. 15, 2015. Cited on page 15.

FLEISCHER, J.; PABST, R.; KELEMEN, S. Heat flow simulation for dry machining of power train castings. *CIRP Annals-Manufacturing Technology*, Elsevier, v. 56, n. 1, p. 117–122, 2007. Cited 3 times on pages 7, 8, and 66.

- GOSSELIN, L.; TYE-GINGRAS, M.; MATHIEU-POTVIN, F. Review of utilization of genetic algorithms in heat transfer problems. *International Journal of Heat and Mass Transfer*, Elsevier, v. 52, n. 9, p. 2169–2188, 2009. Cited on page 16.
- HUSSAIN, M.; TARAMAN, K.; FILIPOVIC, A.; GARRN, I. Experimental study to analyze the workpiece surface temperature in deep hole drilling of aluminum alloy engine blocks using mql technology. *Journal of Achievements in Materials and Manufacturing Engineering*, v. 31, n. 2, p. 485–490, 2008. Cited on page 7.
- ISLAM, C.; LAZOGLU, I.; ALTINTAS, Y. A three-dimensional transient thermal model for machining. *Journal of Manufacturing Science and Engineering*, American Society of Mechanical Engineers, v. 138, n. 2, p. 021003, 2016. Cited on page 10.
- JAEGER, J. Moving heat sources and friction temperature. In: *Proc. Roy. Soc. NSW*. [S.l.: s.n.], 1942. v. 76, p. 203–224. Cited on page 9.
- KAKADE, N.; CHOW, J. Finite element analysis of engine bore distortions during boring operation. *TRANSACTIONS-AMERICAN SOCIETY OF MECHANICAL ENGINEERS JOURNAL OF ENGINEERING FOR INDUSTRY*, AMERICAN SOCIETY MECHANICAL ENGINEERS, v. 115, p. 379–379, 1993. Cited on page 14.
- KARPAT, Y.; ÖZEL, T. Predictive analytical and thermal modeling of orthogonal cutting process—part i: predictions of tool forces, stresses, and temperature distributions. *Journal of manufacturing science and engineering*, American Society of Mechanical Engineers, v. 128, n. 2, p. 435–444, 2006. Cited on page 10.
- KENNEDY, J.; EBERHART, R. Particle swarm optimization. In: *Proceedings of 1995 IEEE International Conference on Neural Networks*. [S.l.: s.n.], 1995. p. 1942–1948. Cited on page 17.
- KENNEDY, J.; KENNEDY, J. F.; EBERHART, R. C.; SHI, Y. *Swarm intelligence*. [S.l.]: Morgan Kaufmann, 2001. Cited on page 17.
- KITAGAWA, T.; KUBO, A.; MAEKAWA, K. Temperature and wear of cutting tools in high-speed machining of inconel 718 and ti 6al 6v 2sn. *Wear*, Elsevier, v. 202, n. 2, p. 142–148, 1997. Cited on page 15.
- KLOCKE, F. *Fertigungsverfahren 2*. [S.l.: s.n.], 2005. Cited 2 times on pages 5 and 8.
- KOMANDURI, R.; HOU, Z. B. Thermal modeling of the metal cutting process: part i—temperature rise distribution due to shear plane heat source. *International Journal of Mechanical Sciences*, Elsevier, v. 42, n. 9, p. 1715–1752, 2000. Cited on page 10.
- KÖNIG, U.; FERTIGUNGSVERFAHREN, B. 1, drehen, fräsen, bohren (reihe studium und praxis) 3 neubearb. *Auflage, Düsseldorf, VDI-Verlag*, 1990. Cited on page 6.
- KUZU, A.; BERENJI, K. R.; EKIM, B.; BAKKAL, M. The thermal modeling of deep-hole drilling process under mql condition. *Journal of Manufacturing Processes*, Elsevier, v. 29, p. 194–203, 2017. Cited on page 13.
- LAURO, C. H.; BRANDÃO, L. C.; VALE, T. J. S.; CHRISTÓFORO, A. L. An approach to define the heat flow in drilling with different cooling systems using finite element analysis. *Advances in Mechanical Engineering*, SAGE Publications Sage UK: London, England, v. 5, p. 612747, 2013. Cited on page 7.

- LAZOGLU, I.; POULACHON, G.; RAMIREZ, C.; AKMAL, M.; MARCON, B.; ROSSI, F.; OUTEIRO, J.; KREBS, M. Thermal analysis in ti-6al-4v drilling. *CIRP Annals-Manufacturing Technology*, Elsevier, 2017. Cited on page 12.
- LI, Z.; QU, X. L. The novel parameter selection of particle swarm optimization. In: TRANS TECH PUBL. *Advanced Materials Research*. [S.l.], 2012. v. 479, p. 344–347. Cited on page 18.
- LIU, F.-B. Particle swarm optimization-based algorithms for solving inverse heat conduction problems of estimating surface heat flux. *International Journal of Heat and Mass Transfer*, Elsevier, v. 55, n. 7, p. 2062–2068, 2012. Cited on page 17.
- LU, S.; HENG, Y.; MHAMDI, A. A robust and fast algorithm for three-dimensional transient inverse heat conduction problems. *International Journal of Heat and Mass Transfer*, Elsevier, v. 55, n. 25, p. 7865–7872, 2012. Cited on page 16.
- MACEDO, S. E. M. *Thermoelastische Verformungen von Werkstücken aus Leichtmetall bei der Trockenbearbeitung*. [S.l.]: Apprimus Verlag, 2015. Cited on page 15.
- OZISIK, M. N. *Inverse heat transfer: fundamentals and applications*. [S.l.]: CRC Press, 2000. Cited on page 16.
- PONTES, D. W. *DETERMINAÇÃO NUMÉRICO EXPERIMENTAL DO COEFICIENTE DE CONVECÇÃO FORÇADA DO FLUIDO DE CORTE APLICADO A USINAGEM POR FURAÇÃO*. Dissertação (Mestrado) — Universidade do Estado de Santa Catarina, 2017. Cited on page 7.
- RAPIER, A. A theoretical investigation of the temperature distribution in the metal cutting process. *British Journal of Applied Physics*, IOP Publishing, v. 5, n. 11, p. 400, 1954. Cited 2 times on pages 10 and 11.
- SATO, M.; AOKI, T.; TANAKA, H.; TAKEDA, S. Variation of temperature at the bottom surface of a hole during drilling and its effect on tool wear. *International Journal of Machine Tools and Manufacture*, Elsevier, v. 68, p. 40–47, 2013. Cited on page 6.
- SEGURAJAUREGUI, U.; ARRAZOLA, P. J. Heat-flow determination through inverse identification in drilling of aluminium workpieces with mql. *Production Engineering*, Springer, v. 9, n. 4, p. 517–526, 2015. Cited 2 times on pages 9 and 66.
- SHAW, M. C.; COOKSON, J. *Metal cutting principles*. [S.l.]: Oxford university press New York, 2005. v. 2. Cited on page 5.
- SHI, Y.; EBERHART, R. A modified particle swarm optimizer. In: IEEE. *Evolutionary Computation Proceedings, 1998. IEEE World Congress on Computational Intelligence., The 1998 IEEE International Conference on*. [S.l.], 1998. p. 69–73. Cited on page 18.
- SHI, Y.; EBERHART, R. C. Empirical study of particle swarm optimization. In: IEEE. *Evolutionary Computation, 1999. CEC 99. Proceedings of the 1999 Congress on*. [S.l.], 1999. v. 3. Cited on page 18.
- SOKOVIĆ, M.; MIJANOVIĆ, K. Ecological aspects of the cutting fluids and its influence on quantifiable parameters of the cutting processes. *Journal of Materials Processing Technology*, Elsevier, v. 109, n. 1, p. 181–189, 2001. Cited 2 times on pages 1 and 7.

- STORN, R. On the usage of differential evolution for function optimization. In: IEEE. *Fuzzy Information Processing Society, 1996. NAFIPS., 1996 Biennial Conference of the North American.* [S.l.], 1996. p. 519–523. Cited on page 26.
- SYSTEMES, D. Abaqus theory manual (6.12). *Dassault Systemes Simulia Corp., Providence, RI, Last accessed Nov*, v. 9, p. 2013, 2013. Cited on page 27.
- TAI, B. L.; STEPHENSON, D. A.; SHIH, A. J. An inverse heat transfer method for determining workpiece temperature in minimum quantity lubrication deep hole drilling. *Journal of Manufacturing Science and Engineering*, American Society of Mechanical Engineers, v. 134, n. 2, p. 021006, 2012. Cited 5 times on pages 13, 14, 34, 35, and 65.
- TAI, B. L.; STEPHENSON, D. A.; SHIH, A. J. Workpiece temperature during deep-hole drilling of cast iron using high air pressure minimum quantity lubrication. *Journal of Manufacturing Science and Engineering*, American Society of Mechanical Engineers, v. 135, n. 3, p. 031019, 2013. Cited on page 35.
- TAY, A. A review of methods of calculating machining temperature. *Journal of Materials Processing Technology*, Elsevier, v. 36, n. 3, p. 225–257, 1993. Cited 3 times on pages 1, 9, and 11.
- TAY, A.; STEVENSON, M.; DAVIS, G. D. V. Using the finite element method to determine temperature distributions in orthogonal machining. *Proceedings of the institution of mechanical engineers*, SAGE Publications, v. 188, n. 1, p. 627–638, 1974. Cited on page 11.
- TAYLOR, F. W. On the art of cutting metals. New York, The American Society of Mechanical Engineers,[1907], 1907. Cited on page 8.
- TRELEA, I. C. The particle swarm optimization algorithm: convergence analysis and parameter selection. *Information processing letters*, Elsevier, v. 85, n. 6, p. 317–325, 2003. Cited on page 18.
- ULUTAN, D.; LAZOGLU, I.; DINC, C. Three-dimensional temperature predictions in machining processes using finite difference method. *Journal of materials processing technology*, Elsevier, v. 209, n. 2, p. 1111–1121, 2009. Cited on page 10.
- VAKILI, S.; GADALA, M. Effectiveness and efficiency of particle swarm optimization technique in inverse heat conduction analysis. *Numerical Heat Transfer, Part B: Fundamentals*, Taylor & Francis, v. 56, n. 2, p. 119–141, 2009. Cited on page 16.
- WEINER, J. Shear-plane temperature distribution in orthogonal cutting. *Trans. ASME*, v. 77, n. 8, p. 1331–1338, 1955. Cited on page 11.
- WEINERT, K.; INASAKI, I.; SUTHERLAND, J.; WAKABAYASHI, T. Dry machining and minimum quantity lubrication. *CIRP Annals-Manufacturing Technology*, Elsevier, v. 53, n. 2, p. 511–537, 2004. Cited on page 1.
- ZEILMANN, R. P. et al. Furação da liga de titânio ti6a14v com mínimas quantidades de fluido de corte. Florianópolis, SC, 2003. Cited on page 6.